Sonic Hedgehog Activates Prostaglandin Signaling to Stabilize Primary Cilium Length

Shariq S. Ansari[1], Miriam E. Dillard[1], Yan Zhang[1], Mary Ashley Austria[1,2], Naoko Boatwright[3], Elaine L. Shelton[3,4], Amanda Johnson[5], Brandon M. Young[6], Zoran Rankovic[6], John D. Schuetz[7], Camenzind G. Robinson[5], and Stacey K. Ogden[1]

[1]Department of Cell and Molecular Biology, [5]Cell and Tissue Imaging Center, [6]Department of Chemical Biology and Therapeutics, [7]Department of Pharmaceutical Sciences, St. Jude Children's Research Hospital, Memphis, TN 38105

[3]Department of Pediatrics, Monroe Carell Jr. Children's Hospital at Vanderbilt and Vanderbilt University Medical Center, [4]Department of Pharmacology, Vanderbilt University School of Medicine, Nashville, TN 37232

[2]Rhodes College Summer Plus Program, Memphis, TN 38112

Correspondence: Stacey.Ogden@stjude.org

ABSTRACT

Sonic Hedgehog (SHH) signaling is an essential driver of embryonic patterning that, when corrupted, leads to developmental disorders and cancers. SHH effector responses are organized through nonmotile primary cilia that grow and retract with the cell cycle and in response to distinct extracellular cues. Destabilization of primary cilium length corrupts SHH pathway regulation, which places significant pressure on SHH to maintain ciliary architecture. Herein, we investigate whether SHH signaling promotes ciliary length control. We reveal a signal crosstalk circuit induced by SHH activation of Phospholipase A2 ($cPLA_2$) that drives ciliary EP_4 signaling to stabilize primary cilium length. We demonstrate that chemical or genetic blockade of SHH-EP_4 crosstalk leads to destabilized primary cilium cyclic AMP (cAMP) control, reduced ciliary length, and attenuated SHH pathway induction. Accordingly, we find that *Ep*$_4^{-/-}$ mice display shortened neuroepithelial primary cilia and altered SHH-dependent neuronal cell fate specification. Thus, SHH initiates a signaling crosstalk circuit that maintains primary cilium length for a robust downstream signaling response.

INTRODUCTION

During embryonic patterning, Sonic Hedgehog (SHH) signaling proteins provide instructional cues that guide cell fate decisions to organize tissues. Disruption of SHH pathway activation leads to developmental disorders and, consistent with regulated signaling being important for tissue homeostasis post-development, aberrant SHH activity drives cancer (Barakat et al., 2010). As such, sophisticated regulatory mechanisms are in place to ensure appropriate pathway control in both basal and activated signaling states. Tight regulation of pathway activity requires localization of SHH pathway components to a specialized sensory organelle called the primary cilium (Caspary et al., 2007; Huangfu and Anderson, 2006). Each cell possesses a single primary cilium that is anchored to the basal body and allows for organization of numerous

signal transduction cascades to instruct diverse cellular responses (Anvarian et al., 2019; Wheway et al., 2018). Despite the membrane of the primary cilium being contiguous with the plasma membrane, it maintains a distinct membrane lipid composition through action of lipid metabolic enzymes that localize near the ciliary base (Arensdorf et al., 2017; Findakly et al., 2021; Garcia et al., 2018; Raleigh et al., 2018). Further, a cytoplasmic diffusion barrier controls entry of soluble proteins into the ciliary body, ensuring that primary cilia offer protected environments for interpretation and transduction of myriad extracellular signals (Garcia et al., 2018; Shi et al., 2017; Ye et al., 2013).

The SHH receptor Patched (PTCH), signal transducer Smoothened (SMO), and GLI2/GLI3 transcriptional effectors all function at or cycle through primary cilia in ligand-regulated manners (Arensdorf et al., 2016; Petrov et al., 2017). In the absence of SHH, SMO retention in primary cilia is restricted by PTCH-mediated depletion of SMO-activating sterols from ciliary membrane (Kinnebrew et al., 2019; Kinnebrew et al., 2021; Kong et al., 2019). In this off state, phosphorylation of GLI2 and GLI3 transcription factors by cyclic AMP (cAMP)-dependent protein kinase (PKA) in primary cilia tags them for partial degradation to remove their transcriptional activation domains (Bangs and Anderson, 2017; Haycraft et al., 2005; Tuson et al., 2011). SHH binding to PTCH attenuates PTCH-mediated ciliary sterol elimination, which leads to SMO sterol binding and retention in primary cilia where it signals to block PKA-promoted GLI truncation. This allows for accumulation of full-length GLI2/3 proteins that are subsequently activated for nuclear translocation and target gene induction (Niewiadomski et al., 2014; Umberger and Ogden, 2021).

67 Current models suggest dependency of SHH signaling on primary cilia evolved due to the
68 specialized lipid composition of ciliary membrane allowing for tight control over availability of
69 SMO-activating sterols (Kinnebrew et al., 2019; Kinnebrew et al., 2021; Kong et al., 2019;
70 Raleigh et al., 2018). Further, the small size of primary cilia allows for rapid modulation of
71 second messengers such as cAMP (Hansen et al., 2020; Truong et al., 2021). Consistent with
72 this functionality and the key role of PKA in regulating GLI that cycles through primary cilia, SHH
73 signal output is highly sensitive to changes in ciliary cAMP concentration (Mukhopadhyay et al.,
74 2013; Truong et al., 2021; Vuolo et al., 2015). Pathway activation lowers primary cilium cAMP to
75 reduce PKA activity by stimulating ciliary exit of $G\alpha_s$-coupled GPR161 (Mukhopadhyay et al.,
76 2013). In addition, SMO can activate heterotrimeric G proteins of the $G\alpha_i$ family to inhibit
77 adenylyl cyclase (AC), suggesting that high-level activation of SHH signaling can lead to
78 sustained reduction in primary cilium cAMP (Barzi et al., 2011; Ogden et al., 2008; Riobo and
79 Manning, 2007).

80

81 Paradoxically, a growing body of evidence supports that ciliary length stability requires high
82 ciliary cAMP. Studies in zebrafish demonstrate that Multidrug Resistance Protein 4 Transporter
83 (ABCC4), which exports the prostaglandin signaling molecule PGE_2, is required for motile cilium
84 elongation. Ciliary length is regulated by PGE_2 activation of the ciliary G protein coupled
85 receptor (GPCR) E-type prostanoid receptor 4 (EP_4) (Jin et al., 2014; Marra et al., 2019). Active
86 EP_4 stimulates $G\alpha_s$ heterotrimeric G proteins, which raise intraciliary cAMP to promote
87 anterograde intraflagellar transport (IFT) for motile cilium length maintenance (Besschetnova et
88 al., 2010; Hansen et al., 2020; Hansen et al., 2022; Jin et al., 2014). Primary cilium length
89 control likely occurs through similar mechanisms because reduced ABCC4 activity in cultured
90 fibroblasts leads to primary cilium shortening and increasing ciliary cAMP leads to primary cilium
91 elongation (Besschetnova et al., 2009; Jin et al., 2014). This raises the possibility that ciliary

92 cAMP reduction in response to high-level activation of SHH signaling could slow IFT, shorten
93 primary cilia, and blunt the downstream signal response. The fail-safes that prevent ciliary
94 shortening in SHH-stimulated cells have not been described.

95

96 We previously reported that SHH activates cytosolic phospholipase A2α ($cPLA_2$) through SMO
97 activation of Gβγ to produce arachidonic acid. Arachidonic acid drives a feed-forward signal that
98 enhances SMO ciliary enrichment such that inhibition of $cPLA_2$ attenuates agonist-induced SMO
99 ciliary accumulation and blunts signaling to GLI transcription factors (Arensdorf et al., 2017).
100 Notably, arachidonic acid can be metabolized to generate the EP_4 agonist PGE_2. This suggests
101 that, in addition to enhancing SMO ciliary enrichment, SHH-mediated production of arachidonic
102 acid may connect the SHH pathway with PGE_2/EP_4-regulated primary cilium length control.
103 Herein, we investigate this hypothesis and reveal a crosstalk circuit between SHH and
104 prostaglandin signaling pathways. We report that SHH-stimulated production of arachidonic acid
105 drives ciliary length homeostasis through production of PGE_2 and activation of EP_4. This
106 provides a mechanism by which ciliary cAMP levels are stabilized in SHH-stimulated cells to
107 sustain anterograde IFT and prevent primary cilium shortening. We show that genetic ablation
108 or small molecule inhibition of SHH-to-EP_4 crosstalk destabilizes primary cilium cAMP
109 concentration, slows IFT, shortens primary cilia, reduces SMO ciliary enrichment, and
110 attenuates SMO signaling to GLI. Consistent with EP_4 signaling being crucial for regulated SHH
111 pathway activation *in vivo*, we find that mice lacking EP_4 have shortened primary cilia and
112 exhibit neural tube patterning defects indicative of compromised SHH signaling. As such, we
113 propose the SHH pathway evolved to link with prostaglandin signaling through $cPLA_2$ activation
114 to stabilize primary cilium length for optimal function of the organelle from which it instructs
115 downstream signaling.

116

117 **RESULTS**

118 *$cPLA_2$ contributes to ciliary length control downstream of SHH.*

119 To determine whether SHH activation of $cPLA_2$ leads to secretion of PGE_2 that regulates
120 primary cilium morphology, we turned to murine kidney inner medullary collecting duct (IMCD3)
121 cells. IMCD3 cells are SHH responsive, produce long primary cilia, and provide an established
122 model for examination of ciliary biology (Breslow et al., 2018; May et al., 2021; Ott and
123 Lippincott-Schwartz, 2012; Zhou et al., 2014). IMCD3 cells were stimulated with control
124 conditioned media or conditioned media containing the amino-terminal signaling domain of SHH
125 for ~24 hours, and then media was collected to test for accumulation of PGE_2. Enzyme-linked
126 immunosorbent assays (ELISA) of conditioned media from control and ligand-treated IMCD3
127 cells showed that SHH stimulated release of PGE_2 and that release was blocked by
128 pretreatment with the inverse SMO agonist cyclopamine. SHH-stimulated PGE_2 secretion was
129 also blocked by pre-treatment with the specific $cPLA_2$ inhibitor giripladib (GIRI) (Figure 1A)
130 (Arensdorf et al., 2017; Duvernay et al., 2015). To determine whether PGE_2 secretion occurred
131 in an ABCC4-dependent manner, we measured release from control or *Abcc4* knockout NIH-
132 3T3 cells following SHH stimulation. Similar to what was observed with IMCD3 cells, SHH
133 stimulation of control NIH-3T3 cells induced secretion of PGE_2 into cell culture medium. This
134 secretion was blocked by inhibiting SMO with cyclopamine or by inhibiting the cyclooxygenase
135 (COX) responsible for initiating arachidonic acid to PGE_2 conversion (Figure 1A', Coxib).
136 Consistent with ABCC4 secreting PGE_2 that is generated in response to SHH pathway
137 activation, *Abcc4* knockout NIH-3T3 cells failed to release prostaglandin in response to SHH
138 treatment (Figure 1A', light gray vs. dark gray). As such, arachidonic acid produced downstream
139 of SHH-stimulated $cPLA_2$ provides a substrate for PGE_2 production and secretion.

140

141 Having established that SHH-mediated $cPLA_2$ activation stimulates PGE_2 release from IMCD3
142 and NIH-3T3 cells, we next evaluated the effect of reducing $cPLA_2$-generated arachidonic acid
143 on ciliary length. We treated IMCD3 cells with vehicle or GIRI in the absence and presence of
144 SHH, and measured lengths of acetylated α-tubulin-marked primary cilia. We generated
145 maximum projections of Z stack images, and then traced the length of each acetylated α-tubulin
146 marked cilium from base to the tip using the line profile tool in LAS X software. GIRI treatment of
147 IMCD3 cells shortened primary cilia significantly, independent of SHH stimulation status.
148 Primary cilium length averaged ~5 μm in the absence of GIRI and shortened by approximately
149 40% to ~3 μm at the highest GIRI concentration used (Figure 1B-C). Ciliary lengths of GIRI-
150 treated cells were rescued by addition of supplemental PGE_2 or its precursor arachidonic acid
151 (Figure 1D-G). Notably, supplemental arachidonic acid augmented ciliary length in SHH-
152 stimulated cells in the absence of GIRI, further supporting a link between increased arachidonic
153 acid availability and primary cilium elongation (Figure 1G, column 2 vs. 3-4). Taken together,
154 these results support that ciliary shortening observed in GIRI-treated cells was a specific effect
155 of compromised arachidonic acid-to-PGE_2 metabolism.

156

157 To determine whether the ciliary morphology changes that occurred following $cPLA_2$ inhibition
158 correlated with reduced SMO ciliary accumulation in IMCD3 cells, we stimulated with SHH
159 conditioned media in the absence or presence of GIRI and quantified SMO ciliary signal
160 intensity (Supplementary Figure 1A-E'). Consistent with what we previously reported for NIH-
161 3T3 cells (Arensdorf et al., 2017), $cPLA_2$ inhibition disrupted SMO ciliary retention in SHH-
162 treated cells (Supplementary Figure 1A-E, red). SHH-stimulated ciliary exit of GPR161
163 (magenta) and retention of the primary cilium resident protein ARL13B (green) were unaffected

164 by GIRI treatment (Supplementary Figure 1A-D, E'), suggesting specificity in the ciliary functions
165 affected by $cPLA_2$ inhibition.

166

167 *EP_4 activation promotes ciliary length homeostasis for SHH signaling to GLI.*

168 Based on established connections between prostaglandin signaling and motile cilia elongation
169 (Jin et al., 2014; Marra et al., 2019), we hypothesized PGE_2 produced downstream of SHH
170 signals through ciliary EP_4 to influence primary cilium length. We therefore sought to determine
171 whether EP_4 localized to primary cilia of IMCD3 cells. EP_4 was evident in primary cilia of both
172 IMCD3 cells and control mouse embryonic fibroblasts (MEF) and was undetectable in cilia of
173 *$Ep_4^{-/-}$* MEFs. These results support specificity of the EP_4 antibody signal and demonstrate that
174 EP_4 localizes to primary cilia in both MEFs and IMCD3 cells (Figure 2A-C').

175

176 To test for EP_4 contributions to primary cilium length maintenance, average ciliary lengths were
177 calculated in control and SHH-treated IMCD3 cells exposed to vehicle or the high-affinity EP_4
178 inhibitor, L161,982 (Cherukuri et al., 2007). Primary cilia of IMCD3 cells treated with increasing
179 concentrations of L161,982 shortened in a dose-dependent manner in the absence of SHH.
180 Notably, ciliary shortening of cells treated with low-dose L161,982 was significantly enhanced by
181 SHH treatment (Figure 2D), demonstrating that an active SHH pathway disrupts primary cilium
182 length control if EP_4 activity is compromised. Supplementing culture media of L161,982-treated
183 cells with high concentrations of the EP_4 ligand PGE_2 partially rescued ciliary length of SHH-
184 stimulated cells, supporting that primary cilium shortening following L161,982 treatment was a
185 specific effect of on-target inhibitor activity toward EP_4 (Figure 2E).

186

187 Having determined that EP_4 contributes to ciliary length maintenance in SHH-stimulated cells,
188 we next wanted to understand how EP_4 inhibition affected SHH signaling output. Thus, SHH-
189 stimulated SMO ciliary signal intensity was quantified in control, GIRI-treated, and L161,982-
190 treated IMCD3 cells. Similar to what we observed following $cPLA_2$ inhibition with GIRI, inhibition
191 of EP_4 with L161,982 attenuated ciliary accumulation of endogenous SMO following SHH
192 exposure (Figure 3A-B and Supplementary Figure 1). Ciliary shortening and reduced SMO
193 accumulation relative to control were also observed in *Ep4*$^{-/-}$ MEFs (Figure 3C-E), further
194 supporting on-target activity of L161,982 to EP_4. To determine whether reduced SMO ciliary
195 enrichment following EP_4 inhibition compromised activation of GLI transcriptional effectors,
196 qPCR analyses of SHH transcriptional targets *Gli1* and *Ptch1* were performed in IMCD3 and
197 NIH-3T3 cells. Inhibition of either $cPLA_2$ with GIRI or EP_4 with L161,982 significantly reduced
198 the ability of SHH to activate a transcriptional response (Figure 3F-F'). Thus, compromised
199 PGE_2/EP_4 signaling shortens cilia and attenuates SHH pathway activity.

200

201 *EP_4 signaling stimulates ciliary cAMP recovery following SHH pathway activation.*

202 We hypothesized that the ciliary length reduction and SHH signal attenuation observed following
203 EP_4 inhibition resulted from altered ciliary cAMP regulation (Figure 4A). To address this
204 hypothesis, we first tested whether reduced ciliary cAMP would lead to shortening of IMCD3
205 primary cilia by knocking down expression of ciliary adenylyl cyclases AC3, AC5, or AC6
206 (Supplementary Figure 2A-B). Consistent with these ACs localizing to primary cilia, their
207 knockdown did not prevent forskolin-stimulated accumulation of whole cell cAMP by cytoplasmic
208 ACs (Supplementary Figure 1C). To specifically measure IMCD3 cell ciliary cAMP following AC
209 knockdown, we used a primary cilium-localized fluorescent sensor system to track ciliary cAMP
210 changes in real time (Supplementary Figure 2D-F'). The sensor revealed that knockdown of

211 each of the ciliary ACs attenuated ciliary cAMP increase by the AC stimulating drug forskolin
212 (Figure 4B). Consistent with reduced ciliary cAMP leading to ciliary shortening, we observed a
213 significant decrease in average IMCD3 cell primary cilium length following knockdown of *Adcy3*,
214 *Adcy5*, or *Adcy6* (Figure 4C). Consistent with reduced primary cilium length compromising the
215 SHH signal response, *Gli1* induction was attenuated following ciliary AC knockdown (Figure
216 4D), suggesting that sustained depletion of ciliary cAMP can compromise ligand-stimulated
217 SHH pathway induction.

218

219 Despite the established link between ciliary length destabilization and reduced SHH pathway
220 activation (Caspary et al., 2007; He et al., 2014), our observation that decreased ciliary cAMP
221 correlated with reduced *Gli1* induction was curious. This is because reduced ciliary AC
222 localization following loss of the ciliary AC chaperone protein ANKMY2 has been shown to
223 induce GLI gain-of-function phenotypes *in vivo* (Somatilaka et al., 2020). To query this
224 discrepancy, we knocked down *Ankmy2* in IMCD3 cells to probe effects of combined ciliary AC
225 depletion on primary cilium cAMP concentration and length control. Consistent with published
226 results, *Ankmy2* knockdown reduced ciliary enrichment of endogenous AC3 and AC5/6
227 (Somatilaka et al., 2020) and blocked the ability of forskolin to trigger rapid ciliary cAMP
228 accumulation (Supplementary Figure 3A-D). To determine how ciliary AC depletion impacted
229 primary cilium length and SHH pathway induction, we measured primary cilia and performed
230 *Gli1* qPCR analyses in control and *Ankmy2* knockdown cells treated with control or SHH
231 conditioned media. Notably, *Ankmy2* knockdown triggered a 23% reduction in IMCD3 cell
232 primary cilium length and attenuated SHH-stimulated *Gli1* induction (Figure 4E-F). These results
233 suggest the inability of cells to raise ciliary cAMP in SHH-stimulated cells compromises the
234 ligand-induced transcriptional response.

235

236 To further evaluate this hypothesis, we next probed effects of ciliary AC depletion on the SHH
237 response in highly SHH-responsive NIH-3T3 cells. Due to baseline primary cilia lengths in NIH-
238 3T3 cells being shorter than those of IMCD3 cell cilia, length reductions occurring in response to
239 ciliary AC depletion were difficult to appreciate. Nevertheless, we observed that knockdown of
240 *Adcy5* or *Ankmy2* led to modest, but statistically significant, reduction in primary cilium lengths
241 in NIH-3T3 cells (Supplementary Figure 3E-F). *Adcy3* knockdown did not alter NIH-3T3 ciliary
242 length, suggesting AC5 may be the primary modulator of cAMP-mediated primary cilium length
243 regulation in this cell type (Supplementary Figure 3F). Accordingly, and consistent with
244 published results (Somatilaka et al., 2020), we observed that knockdown of *Ankmy2* significantly
245 reduced SHH-stimulated *Gli1* induction in NIH-3T3 cells (Supplementary Figure 3G). Consistent
246 with *Ankmy2* knockdown leading to a pan-AC ciliary depletion, individual knockdown of either
247 *Adcy3* or *Adcy5* attenuated the SHH transcriptional response to a lesser extent than *Ankmy2*
248 knockdown (Supplementary Figure 3G). We did not detect endogenously expressed *Adcy6*
249 transcript in NIH-3T3 cells, so did not test knockdown of *Adcy6* in this cell type. These results,
250 combined with the results presented above, lead us to conclude that primary cilium AC
251 depletion is detrimental to the ligand-induced SHH signal response.

252

253 Having established that lowering ciliary cAMP by AC depletion appreciably and significantly
254 shortened primary cilia and attenuated SHH signaling in IMCD3 and NIH-3T3 cells, we next
255 sought to determine whether cAMP dynamics downstream of SMO activation were impacted by
256 EP_4. Thus, IMCD3 cells were stimulated with the AC activator forskolin, and ciliary cAMP was
257 monitored in control and SMO stimulated cells using the fluorescent cAMP system introduced
258 above. As anticipated, forskolin treatment stimulated a rapid increase in ciliary cAMP

259 fluorescence intensity ratios (Figure 5A, red and Supplementary Figure 2F-F', blue). Consistent
260 with the ability of activated SMO to couple with $G\alpha_i$ and induce exit of $G\alpha_s$-coupled GPR161
261 from primary cilia, co-stimulation of IMCD3 cells with forskolin and the direct SMO agonist SAG
262 reduced the level to which forskolin could raise ciliary cAMP. Despite this, ciliary cAMP in cells
263 treated with forskolin + vehicle and forskolin + SAG equilibrated similarly after an initial lag
264 (Figure 5A, red vs blue). We hypothesized cAMP equilibration was the result of EP_4 activation
265 downstream of SMO-stimulated PGE_2 release. Accordingly, ciliary cAMP equilibration in SAG-
266 stimulated cells was blocked by direct EP_4 inhibition with L161,982 (Figure 5A, green vs. blue).
267 We conclude EP_4 activation is required to equilibrate primary cilium cAMP levels in cells with an
268 active SHH signaling pathway.

269

270 Previous reports indicate that activation of EP_4 raises cAMP to promote anterograde IFT
271 (Besschetnova et al., 2010; Jin et al., 2014). To determine if this activity was compromised by
272 EP_4 inhibition in SHH-stimulated cells, we calculated anterograde velocity of the ciliary
273 intraflagellar transport protein IFT88 in control and L161,982-treated cells. We observed
274 increased anterograde IFT in vehicle-treated, SHH-stimulated cells (Figure 5B, lane 1 vs. 2).
275 Strikingly, anterograde IFT88 velocity was significantly reduced following treatment with the EP_4
276 inhibitor L161,982 in both control and SHH-stimulated IMCD3 cells (Figure 5B). Thus, EP_4
277 activity is required to maintain anterograde IFT in control cells and enhance its velocity in SHH-
278 stimulated cells.

279

280 If cAMP equilibration that stabilizes primary cilium length in SHH-stimulated cells occurs through
281 SHH-to-EP_4 crosstalk, we reasoned that providing supplemental ciliary cAMP might restore
282 ciliary length to rescue SHH pathway induction in L161,982-treated cells. To affect ciliary cAMP

283 in a controlled manner, we adapted a published optogenetic system (Truong et al., 2021) for
284 use in IMCD3 cells. In this system, bacterial photoactivatable adenylyl cyclase (bPAC) is
285 expressed in the cell cytoplasm or targeted to primary cilia through fusion with the primary
286 cilium-localized protein ARL13B, and then activated to specifically raise cytoplasmic or ciliary
287 cAMP by blue light stimulation (Supplementary Figure 4A). IMCD3 cells were engineered to
288 stably express cytoplasmic or ciliary bPAC-GFP, and then exposed to blue light to quantify
289 primary cilium length changes (Supplementary Figure 4B-C"). IMCD3 cells expressing
290 cytoplasmic or ciliary bPAC proteins showed similar average primary cilium lengths in the
291 absence of blue light and cilia of cyto-bPAC-expressing cells did not change length upon blue
292 light exposure, despite its ability to increase cytoplasmic cAMP levels (Supplementary Figure
293 4C-C'). Conversely, cilia-bPAC-expressing cells increased their average primary cilium length
294 by ~30% upon blue light exposure (Supplementary Figure 4C, C"). To support that elongation
295 resulted from increased primary cilium cAMP, we measured primary cilium lengths in IMCD3
296 cells treated with forskolin, which stimulates both ciliary and non-ciliary AC. We observed an
297 increase in average primary cilium length in forskolin-treated cells that was similar to that
298 observed following cilia-bPAC activation (Supplementary Figure 4D-D'). Thus, small molecule or
299 optogenetic increase in ciliary cAMP can increase primary cilium length.

300

301 Having validated feasibility of using ciliary bPAC to modulate primary cilium cAMP in IMCD3
302 cells, we next determined whether shortened cilia of EP_4-inhibited cells could be reversed by
303 increasing ciliary cAMP. Consistent with the hypothesis that reduced primary cilia lengths in
304 SHH-stimulated L161,982-treated cells resulted from failed cAMP equilibration, blue light
305 stimulation of cilia-bPAC partially rescued average primary cilium length in EP_4-inhibited, SHH-
306 stimulated cells. Blue light stimulation increased average ciliary lengths of L161-982-treated,
307 ciliary-bPAC-expressing cells by ~25% in the absence and presence of SHH (Figure 5C). To

308 test whether ciliary length increase correlated with rescue of SHH pathway activity, we
309 quantified SMO ciliary enrichment in control and blue light-stimulated, cilia-bPAC-expressing
310 cells after L161,982 treatment. Consistent with the ability of blue light-induced cAMP to partially
311 rescue ciliary length following EP_4 inhibition, SHH-stimulated SMO ciliary enrichment was also
312 partially restored in blue light-stimulated, L161,982-treated cilia-bPAC cells (Figure 5D, column
313 3 vs. 6). Intriguingly, SHH-stimulated enrichment of SMO in vehicle-treated cells was enhanced
314 by blue light stimulation, supporting that augmenting cAMP production in cells with an active
315 SHH pathway may enhance anterograde IFT to facilitate increased SMO ciliary enrichment
316 (Figure 5D, column 2 vs. 5). Thus, EP_4-regulated ciliary cAMP control impacts both primary
317 cilium length and SMO ciliary accumulation.

318

319 *EP_4 is required for ciliary length control and SHH signaling during neural tube development.*

320 Having established a cell biological connection between SHH and EP_4 that stabilizes primary
321 cilium length, we next sought to determine whether EP_4 loss compromised ciliary length control
322 to impact SHH signaling *in vivo*. Thus, we analyzed developing neural tubes of *Ep4*$^{-/-}$ mice to
323 assess primary cilium length and evaluate SHH-regulated ventral neural tube cell fate
324 specification. *Ep4*$^{-/-}$ mice are present at normal Mendelian ratios *in utero* but die as neonates
325 due to heart failure resulting from highly penetrant patent ductus arteriosus (Segi et al., 1998).
326 Thus, we collected E9.5/29 somite stage *Ep*$_4^{+/-}$ and *Ep*$_4^{-/-}$ embryos to perform scanning electron
327 microscopy for visualization of apical primary cilia of cells lining the neural tube lumen (Figure
328 6A). Measurement of apical primary cilia revealed statistically significant length reductions in
329 *Ep4*$^{-/-}$ embryos compared to cilia of heterozygous littermate controls (Figure 6B). Whereas
330 primary cilia in control neural tubes averaged ~0.9 μm, cilia in knockout embryos showed an

331 approximate 30% length reduction to an average length of ~0.6 μm. Thus, EP_4 contributes to
332 primary cilium length control in the developing neural tube.

333

334 During neural tube development, SHH signals in a graded manner from the notochord and
335 neural tube floor plate to instruct transcriptional programs that establish ventral neural tube cell
336 fates (Ericson et al., 1997; Patten and Placzek, 2000; Ribes and Briscoe, 2009). To test whether
337 EP_4 loss led to alteration of SHH-dependent neural tube progenitor domain specification, we
338 examined expression of the ventral SHH transcriptional target *Olig2,* which is activated by high
339 SHH, and the intermediate fate marker *Pax6* (Ericson et al., 1997; Ribes and Briscoe, 2009).
340 Because specification of ventral progenitor domains is highly sensitive to SHH signal alteration,
341 monitoring their induction allows for reliable reporting of SHH signaling activity (Ribes and
342 Briscoe, 2009). Comparison of E9.5/27 somite stage knockout and heterozygous littermate
343 control neural tubes revealed that EP_4 loss led to reduction in the *Olig2*-postive motor neuron
344 progenitor cell population, indicative of reduced SHH signaling response in *Ep4*$^{-/-}$ mice.
345 Coincident with reduction in the *Olig2*-expressing progenitor domain, we observed expansion of
346 the *Pax6*-expressing progenitor population (Figure 6C-D). Taken together with the above, these
347 results support that EP_4 loss shortens primary cilia and compromises SHH-directed cell fate
348 specification *in vivo*.

349

350 **DISCUSSION**

351 Prostaglandin signaling is important for motile cilia development and beat frequency and
352 contributes to primary cilium elongation (Gayner and McCaffrey, 1998; Haxel et al., 2001; Jin et
353 al., 2014; Marra et al., 2019). The study presented here reveals the SHH pathway, which
354 requires functional primary cilia to initiate downstream effector responses, links with the PGE_2

355 pathway to ensure ciliary length homeostasis. We delineate a SHH-to-PGE_2/EP_4 signal
356 crosstalk circuit and demonstrate that SHH-stimulated PGE_2 production leads to activation of
357 $G\alpha_s$-coupled EP_4. EP_4 signaling equilibrates ciliary cAMP after an initial dip following SHH/SAG-
358 stimulated ciliary exit of $G\alpha_s$-coupled GPR161 and activation of $G\alpha_i$-coupled SMO. We propose
359 that cAMP equilibration maintains anterograde IFT that is necessary for SMO ciliary enrichment
360 and primary cilium length stability (Figure 7A-B). Genetic or pharmacological interruption of the
361 SHH-to-EP_4 signal crosstalk cascade short-circuits ciliary cAMP equilibration in SHH-stimulated
362 cells, slows anterograde IFT, shortens primary cilia, and attenuates SHH signal output (Figure
363 7C). *In vivo* loss of EP_4 leads to short neuroepithelial primary cilia and neural tube defects
364 indicative of compromised SHH signaling. These results support an essential link between SHH
365 and EP_4 ciliary signaling pathways during embryonic development.

366

367 Although the requirement for functional primary cilia in regulation of SHH signaling is well
368 established, the complex relationship between SHH and cAMP modulation in cilia has yet to be
369 clearly defined. To initiate a transcriptional response, SHH must lower ciliary cAMP to halt PKA-
370 instructed GLI processing into its repressor form (Mukhopadhyay et al., 2013; Niewiadomski et
371 al., 2014). Consistent with this biology, genetic loss of the AC chaperone *Ankmy2* depletes
372 primary cilia of AC activity, attenuates PKA-directed GLI repressor conversion, and allows for
373 unregulated accumulation of full length GLI proteins that induce gain-of-function phenotypes *in*
374 *vivo*. Although ciliary length reduction was not noted in *Ankmy2* knockout mice, mechanistic *in*
375 *vitro* analyses revealed that *Ankmy2* knockout NIH-3T3 cells were, nonetheless, compromised
376 in their ability to induce SHH-stimulated transcriptional responses (Somatilaka et al., 2020). This
377 suggests the ability to precisely tune ciliary cAMP levels up or down is essential for optimal
378 ligand-stimulated SHH pathway activity. Our data suggest SHH-promoted EP_4 signaling is a key
379 mechanism by which up-tuning occurs, and that this crosstalk is necessary to prevent slowing of

380 anterograde IFT and primary cilium shortening that can occur in response to sustained ciliary
381 cAMP depletion. However, the requirement for SHH to activate $G\alpha_s$-coupled EP_4 to stabilize
382 primary cilium length prompts the question of how GLI escapes PKA-mediated repressor
383 conversion upon ciliary cAMP re-elevation. We hypothesize GLI stabilization is maintained in
384 SHH-stimulated cells through direct PKA inhibition by active SMO. Recent reports demonstrate
385 that SHH-stimulated phosphorylation of the intracellular carboxyl-terminal tail of SMO exposes a
386 PKA inhibitory domain (PKI) that prevents GLI phosphorylation (Arveseth et al., 2021; Happ et
387 al., 2022). As such, we propose SHH coordinates a sophisticated ciliary signal response
388 through a network of interconnected GPCR activities.

389

390 Notably, GPCR signal crosstalk downstream of Hedgehog (Hh) family ligands that equilibrates
391 cAMP may be a conserved mechanism by which pathway activity is controlled. In *Drosophila*,
392 Hh-activated Smo stimulates $G\alpha_i$ to lower cAMP and halt PKA-regulated truncation of the GLI
393 ortholog Cubitus interruptus (Ci) (Ogden et al., 2008). However, a *Drosophila*-specific positive
394 regulatory role for PKA-mediated phosphorylation of Smo is required for high-level pathway
395 induction, and could be disrupted by Smo activation of $G\alpha_i$ (Jia et al., 2004). A potential
396 mechanism by which Smo solves this problem was revealed by the discovery that, in some cell
397 types, Smo stimulation leads to $G\alpha_s$ activation to enhance pathway responsiveness to low-
398 threshold Hh stimulation (Praktiknjo et al., 2018). It is not yet clear whether $G\alpha_s$ activation
399 downstream of Hh occurs through Smo signal bias or by Smo crosstalk with $G\alpha_s$-coupled GPCR
400 signaling partners. Nevertheless, the observation that Smo can lead to $G\alpha_s$ activation in flies
401 supports an evolutionarily conserved ability of Hedgehog family members to affect exquisite
402 control of cAMP modulators to ensure appropriate downstream signaling activity.

403 **Table 1: Reagents and Resources**

REAGENT or RESOURCE	SOURCE	IDENTIFIER
Antibodies		
Smoothened	Santa Cruz Biotechnology	sc-166685, RRID:AB2239686
Acetylated α-Tubulin	Cell Signaling	5335S, RRID:AB_0544694
ARL13B	Antibodies Incorporated	75-287, RRID:AB_2341543
EP4	Santa Cruz Biotechnology	sc-55596, RRID:AB_2174775
AC3	Proteintech	19492-1-AP RRID:AB_10638445
AC5/6	FabGennix	PAC-501AP
PAX6	Developmental Studies Hybridoma Bank	RRID:AB_528427
OLIG2	Millipore	AB9610, RRID:AB_570666
GPR161	Saikat Mukhopadhyay	N/A
AlexaFluor 488	Life Technologies	A11029 (Mouse), RRID:AB_2534088; A11034 (Rabbit), RRID:AB_2576217
AlexaFluor 555	Life Technologies	A21424 (Mouse), RRID:AB_141780; A21429 (Rabbit), RRID:AB_2535850
AlexaFluor 647	Life Technologies	A21236 (Mouse), RRID:AB_2535805; A21245 (Rabbit), RRID:AB_2535813
Chemicals, Peptides, and Recombinant Proteins		
Arachidonic Acid	Cayman Chemical Company	90010-50

Giripladib	This Paper	N/A
L161,982	Tocris Chemicals	2514
Prostaglandin E2	Sigma Chemicals	P5640
Cyclopamine	LC Laboratories	C-8700
Celecoxib	Cayman Chemical Company	10008672
Forskolin	Sigma Chemicals	F6886-10MG
SAG	Selleck Chemical Company	S7779-2MG
Lipofectamine™ 3000	Thermo Fisher Scientific	L3000008
Lipofectamine™ RNAiMAX	Thermo Fisher Scientific	13778150
IBMX	Sigma-Aldrich	I5879-1G
DMSO	Sigma-Aldrich	D2650
Hygromycin	Life Technologies	10687010
PowerUp SYBR Green Master Mix	Applied Biosystems	A25742
Commercial Assay Kits		
Prostaglandin E2 Parameter Assay Kit	R&D Systems	KGE004B
BCA Protein Assay Kit	Thermo Scientific™ Pierce™	23227
RNeasy Plus Mini Kit	Qiagen	74136
High-Capacity cDNA Reverse Transcription Kit	Applied Biosystems	4368813
Ratio-metric Cilia-Targeted cADDis cAMP	Montana Molecular	D0211G
Direct cAMP ELISA kit	Enzo Life Sciences	ADI900066
Oligonucleotides		
Ptch1 Forward: TCACCTCCATCAGCAATGTC	Thermo Fisher Scientific	N/A
Ptch1 Reverse: GAATACCACCACCACAGCAG	Thermo Fisher Scientific	N/A

Gli1 Forward: CCAAGCCAACTTTATGTCAGGG	Thermo Fisher Scientific	N/A
Gli1 Reverse: AGCCCGCTTCTTTGTTAATTTGA	Thermo Fisher Scientific	N/A
Adcy3 Forward: GCTTTCTTTGTCTTCTCCTTC	Thermo Fisher Scientific	N/A
Adcy3 Reverse: ATGATAGCACACAGGTAGAG	Thermo Fisher Scientific	N/A
Adcy5 Forward: GTCTCAGAAAGTGGCAATTC	Thermo Fisher Scientific	N/A
Adcy5 Reverse: CATTCAGGTAGTTGAGTGTG	Thermo Fisher Scientific	N/A
Anmky2 Forward: GCTGCCAAAACATAAGAGACAG	Thermo Fisher Scientific	N/A
Anmky2 Reverse: CTTCTTTCTCCCTTCCACAG	Thermo Fisher Scientific	N/A
Adcy6 Forward: ACGTTGCCATGGAGATGAAA	Thermo Fisher Scientific	N/A
Adcy6 Reverse: TCAATGTCCGCAAACAGGAT	Thermo Fisher Scientific	N/A
Ppia Forward: AGCACTGGAGAGAAAGGATT	Thermo Fisher Scientific	N/A
Ppia Reverse: ATTATGGCGTGTAAAGTCACCA	Thermo Fisher Scientific	N/A
Btf3 Forward: GAACAACATCTCTGGTATTGAAGA	Thermo Fisher Scientific	N/A
Btf3 Reverse: AATGGTGAAGGTGTTTGCTG	Thermo Fisher Scientific	N/A
Adcy3 siRNA	Thermo Fisher Scientific	Assay ID: S98223
Adcy5 siRNA	Thermo Fisher Scientific	Assay ID: S104765

Adcy6 siRNA	Thermo Fisher Scientific	Assay ID: s104033
Anmky2 siRNA	Thermo Fisher Scientific	Assay ID: MSS235827
Experimental Models: Cell Lines		
IMCD3	ATCC	CRL-2123
IMCD3 Flp-In Cells	Maxence Nachury Lab	N/A
IMCD3 EF1α-Cyto-bPAC-GFP	This Paper	N/A
IMCD3 EF1α-Arl13b-Cilia-bPAC-GFP	This Paper	N/A
NIH-3T3	ATCC	CRL-1658
Abcc4$^{-/-}$ NIH-3T3	John Schuetz lab	N/A
Ep4$^{-/-}$ Mouse Embryonic Fibroblast	This paper	N/A
Wild Type Mouse Embryonic Fibroblast	This paper	N/A
Experimental Models: Mouse Model		
Ep4$^{+/-}$ Mice	Elaine Shelton	(Segi et al., 1998)
Ep4$^{-/-}$ Mice	Elaine Shelton	(Segi et al., 1998)
Recombinant DNA		
pgLAP5-EF1α dTATA-bPAC-GFP	Jeremy Reiter	(Truong et al., 2021)
pgLAP5-EF1α dTATA-Arl13b-bPAC-GFP	Jeremy Reiter	(Truong et al., 2021)
pEF1α-mIFT88-EGFP	Addgene	149697
5HT6-mCherry-G-GECO1.0	Addgene	47500
pcDNA-DEST47-Arl13b-GFP	Addgene	40872
Software and Algorithms		
GraphPad Prism v. 8.2.0	GraphPad Software	http://www.graphgad.com/

ImageJ	NIH software	https://imagej.nih.gov/ij/
LAS X	Leica	
JACoP	Open Source	https://imagej.nih.gov/ij/plugins/track/jacop2.html
KymographDirect v. 2.0	Open Source	https://sites.google.com/site/kymographanalysis/
NIS-Elements Viewer v. 4.50.00	Nikon	https://www.microscope.healthcare.nikon.com/products/software/nis-elements/viewer
Inkscape	Open Source	https://inkscape.org/

404

405 **RESOURCE AVAILABILITY**

406 Requests for resources and reagents should be directed to Stacey K. Ogden
407 (Stacey.Ogden@stjude.org). Cell lines and novel reagents will be available upon request
408 pursuant to SJCRH material transfer agreement.

409

410 **METHODS**

411 *Mammalian Cell culture*

412 Wild type and Flp-In IMCD3 cells were cultured in Dulbecco's Modified Eagle Medium (DMEM):
413 F12 supplemented with 10% fetal bovine serum (FBS) and 1% Penicillin Streptomycin solution
414 (Gibco). Wild type MEFs, NIH-3T3, *Ep4*$^{-/-}$ MEF, and *Abcc4*$^{-/-}$-NIH-3T3, were supplemented with
415 10% fetal calf serum. Cells were passaged routinely with 0.25% Trypsin/EDTA solution and
416 maintained under standard incubation conditions (5% CO_2, 37°C) in a humidified incubator. All
417 cell lines were routinely tested for mycoplasma contamination. To promote ciliogenesis, cell
418 lines were serum starved for 2 hours in serum-free media (DMEM or DMEM: F12,
419 supplemented with 0.1 mM nonessential amino acids, 2mM L-Glutamine, 1mM sodium
420 pyruvate, and 1% Pen-Strep). After starvation, media was replaced with low serum (0.5%)
421 media and cells were incubated for 18 or 36 hours.

422

423 *Chemicals*

424 L161,982 (Tocris), Cyclopamine (LC Laboratories) and Celecoxib (Coxib, Cayman Chemical
425 Company) were reconstituted in DMSO and stored at -20°C. Arachidonic acid (Cayman
426 Chemical Company) was stored in ethanol at -20°C. Prostaglandin E_2 (Sigma Chemicals) and
427 Forskolin (Sigma Chemicals) were reconstituted in ethanol and stored at 4°C. Giripladib (GIRI)

428 was synthesized and stored according to published procedures (Duvernay et al., 2015; Thotala
429 et al., 2013).

430

431 *Immunofluorescence and ciliary length measurement*

432 For cultured cells ciliary analysis, cells were plated onto coverslips (Corning) and pretreated
433 with either vehicle or drug in serum-free media. After 2 hours, media was changed to low serum
434 media containing drug and SHH-N conditioned media (100 µL/mL), and then incubated for ~18
435 hours. After incubation, cells were washed with PBS, and then fixed in 4% paraformaldehyde for
436 12 minutes. Cells were then washed with wash buffer (PBS with 0.1% Triton X-100) three times
437 for 5 minutes and incubated in blocking buffer for 60 minutes at room temperature (PBS with 2%
438 BSA, 0.1% Triton X-100, 1% goat serum). Primary antibody incubations were performed
439 overnight at 4°C. The following antibodies and dilutions were used: anti-SMO (Santa Cruz,
440 1:500), anti-acetylated α-tubulin (Cell Signaling, 1:1000), anti-ARL13B (Antibodies Incorporated,
441 1:500), anti-EP_4 (Santa Cruz, 1:100), anti-AC5/6 (FabGennix, 1:75), anti-AC3 (Proteintech,
442 1:200) diluted in blocking buffer. Secondary antibody incubations were performed with
443 AlexaFluor 488, 555, or 647 conjugated secondary antibodies (Life Technologies, 1:1000) and
444 DAPI for 60 minutes at room temperature. Following antibody incubation, samples were washed
445 three times in wash buffer followed by a rinse in PBS, prior to mounting with ProLong Diamond
446 (Life Technologies). Images were collected using Leica TCS SP8 STED 3x confocal microscope
447 with a 63x oil-immersion objective and processed using LAS X (Leica). For all
448 immunofluorescence experiments, multiple cells (≥100) were examined over at least two
449 independent experiments. Representative images are shown.

450

451 For ciliary length measurement, a maximum projection of the acquired Z stack images was
452 created. Each cilium was manually traced from the base to the tip using the line profile tool in
453 the LAS X software. For all experiments, >100 cilia were measured for each condition across a
454 minimum of two independent experiments. For quantification graphs, all data are included. For
455 microscopy images, representative cilia are shown.

456

457 *In vivo analysis*

458 Data and materials generated from animals were obtained in accordance with SJCRH/IACUC
459 approved protocol 608-100616-10/19 and Vanderbilt protocol M1600016-01. All animal
460 husbandry and procedures were performed in accordance with protocols approved by St. Jude
461 Children's Research Hospital and Vanderbilt University Institutional Animal Care and Use
462 Committees.

463

464 *Ep4*$^{+/-}$ and *Ep4*$^{-/-}$ embryos in the C57BL/6 background were harvested and processed for
465 immunohistochemistry at E9.5. Pregnant dams were harvested, uterine horns removed, and
466 embryos were dissected in 1X PBS, then rinsed three times in 1X PBS. Embryos were fixed
467 overnight at 4°C in 4% PFA. The following day, embryos were rinsed three times in 1X PBS and
468 transferred to 30% sucrose to cryo-protect. The following day, embryos were frozen in O.C.T.
469 Compound (Tissue-Tek) on dry ice. Embryos were sectioned transverse at 15 µm thickness on
470 a Leica Microm CM1950 cryo-stat. Sections were briefly dried, then washed in 1X TBST, then
471 blocked with 2% BSA, 1% goat serum, 0.1% Triton-X-100 in 1X PBS. Antibodies were diluted in
472 blocking buffer and incubated overnight on sections at room temperature. The following
473 antibodies and dilutions were used: mouse anti-PAX6 (1:25; DSHB), and rabbit anti-OLIG2
474 (1:300; Millipore). Primary antibody was removed, sections were washed with 1X TBST three

475 times, then incubated for 3 hours in secondary antibodies (Invitrogen) at a 1:500 dilution.
476 Sections were washed three times in 1X TBST, then rinsed with water, dried, and cover slips
477 were applied with ProLong Gold mounting media with DAPI. Sections were imaged on a Leica
478 DMi8 widefield microscope. A minimum of four embryos per genotype were analyzed.

479

480 To quantify the *Olig2* and *Pax6* expressing domains, at least three sections per embryo in the
481 thoracic region were randomly chosen, and their area was measured using the Segmented Line
482 Tool in ImageJ. The percentage area of each domain was calculated with respect to the entire
483 Dorsal Ventral extent of the neural tube. The data are presented as mean ± SD, and statistical
484 comparisons were made using Student's t-test. GraphPad software was used for statistical
485 analysis. p-values less than 0.05 were considered statistically significant.

486

487 For electron microscopy of neural tube primary cilia, samples were fixed in 2.5% glutaraldehyde,
488 2% paraformaldehyde in 0.1M cacodylate buffer containing 2 mM $MgCl_2$. Following fixation,
489 samples were dissected to expose the interior of the neural tube lumen. Dissected samples
490 were buffer washed, post-fixed in 0.1% aqueous osmium tetroxide for 1 hour, washed with
491 ddH_2O, dehydrated with an ascending ethanol series, and critical point dried in liquid CO_2 using
492 an Autosamdri 931 (Tousimis). Dried samples were sputter-coated under planetary rotation with
493 15 nm iridium and imaged in a ThermoFisher Scientific Teneo scanning electron microscope at
494 2 kV using the Everhart-Thornley and T1 detectors.

495

496 *cAMP measurement*

497 cAMP in whole cell lysates was measured using the Direct cAMP ELISA kit (Enzo). Cells were
498 seeded in 6-well plates at a density of $3.5x10^5$ cells per well. The next day, cells were starved
499 for 2 hours in serum free media followed by overnight incubation in low serum media to promote
500 ciliation. On the day of treatment, cells were treated with 100 μM IBMX diluted in low serum
501 media and scraped into lysis buffer (0.1 M HCl, Enzo). Samples were analyzed per the
502 manufacturer's protocol. cAMP concentrations were calculated using a 4-parameter logistic
503 (4PL) and cAMP concentrations were normalized to the total protein concentrations, determined
504 by a BCA protein assay (Thermo Fisher Scientific).

505

506 *Ciliary cAMP assay*

507 IMCD3 cells were seeded at 18,000 cells/well in an 8-well chamber slide (Nunc™ Lab-Tek™ II
508 Chamber Slide™ System) and transduced the next day with the ratiometric cilia-targeted
509 cADDis BacMam (Montana Molecular, D0211G) per manufacturer's recommendation. Cells
510 were infected with 20 μl of BacMam sensor stock in a total of 250 μl of media containing 2 mM
511 Sodium Butyrate (Molecular Montana) for 30 minutes at room temperature in dark followed by 5
512 hours at 37°C. BacMam was removed and replaced with low serum media containing 1 mM
513 Sodium Butyrate for 16-24 hours with or without vehicle, GIRI, or L-161,982 treatment. Prior to
514 imaging, cells were incubated in PBS for 20 minutes at room temperature. Positive agonist FSK
515 (100 μM) was added 30 seconds after the recording was initiated and images were acquired on
516 a Nikon A1R confocal on live cell imaging mode (63x, epifluorescence) every 10 seconds for 8
517 minutes. For experiments with SAG, the signal was recorded for basal conditions followed by
518 incubation with forskolin for 1.5 minutes and then treated with either SAG or vehicle and
519 recorded every 10 seconds for 8 minutes.

520

521 For knockdown experiments, IMCD3 cells were seeded in 8-well chamber slides (Nunc™ Lab-
522 Tek™ II Chamber Slide™ System) followed by siRNA treatment the next day with either the
523 control siRNA or *Adcy3, Adcy5*, *Adcy6* or *Ankmy2* siRNA. Cells were then transduced the
524 following day with the ratiometric cilia-targeted cADDis BacMam and the experiment was carried
525 out as described above.
526
527 *Generation of optogenetic bPAC cells*
528 IMCD3 cell lines stably expressing Cyto-bPAC-GFP and Cilia-bPAC-GFP were generated using
529 the Flp-In system following manufacturer's instructions (Invitrogen). IMCD3 Flp-In cells (Breslow
530 and Nachury, 2015) were transfected using Lipofectamine 3000 with the appropriate plasmids
531 and selected with 40 mg/mL hygromycin (Gibco). Single colonies were expanded, and protein
532 expression was confirmed by fluorescence microscopy for GFP.
533
534 *Optogenetic stimulation*
535 bPAC-expressing IMCD3 Flp-In cells were plated onto coverslips, grown to confluency, and
536 pretreated with either vehicle or L161-982 (10 μM) in serum-free media. After 2 hours, media
537 was changed to low serum media containing vehicle or drug and SHH-N conditioned media
538 (100 μL/mL), and then incubated for ~18 hours. Prior to immunofluorescence analysis, cells
539 were transferred to a custom-made LED humidified incubator with 5% CO_2 for continuous blue
540 light 450 nm stimulation at ~0.4 mW/cm^2 for 3 hours (Zhang et al., 2019). Following this,
541 immunofluorescence staining was performed as described above.
542
543 *Quantitative Reverse Transcriptase Polymerase Chain Reaction (qRT-PCR)*

544 Total RNA was extracted from cells using the RNeasy Mini Kit (Qiagen) according to
545 manufacturer's protocol. One thousand nanograms of RNA was used to synthesize
546 complementary DNA (cDNA) using High-Capacity cDNA Reverse Transcription Kit (Applied
547 Biosystems). qRT-PCR reactions were performed on a QuantStudio 7 Flex PCR machine using
548 PowerUp Sybr Green Master Mix (Applied Biosystems). Corresponding changes in the
549 expression levels of selected genes were calculated using the ΔΔCt method relative to
550 housekeeping genes, *Ppia* and *Btf3* (Arensdorf et al., 2017).

551

552 *Cell Line Generation*

553 EP_4 knockout cells were generated from *Ep4*$^{-/-}$ embryos (Segi et al., 1998). Embryos (13.5 dpc)
554 were freshly isolated and placed in individual 10 cm culture dishes where they were eviscerated.
555 Heads were removed and used for genotyping to identify homozygous null embryos and wild
556 type littermates using conventional PCR. Embryo bodies were transferred to 15 mL conical
557 tubes containing 5 mL fresh PBS and dissociated by aspirating through a 16G needle into a 10
558 mL syringe and expelling the contents. Warm media (DMEM+10%FBS+1%pen/strep) was then
559 added to each conical tube to bring the total volume to 10 mL. This solution was transferred to a
560 15 cm culture dish containing 25 mL additional media and placed in a 37°C incubator. After 24h,
561 media and non-adherent tissue pieces were removed, and fresh media was added. Cells were
562 grown to 80-90% confluence, after which they were passaged and frozen down after passage
563 number two. *Abcc4*$^{-/-}$ NIH-3T3 cells were generated as previously described (Wijaya et al.,
564 2020).

565

566 *PGE_2 ELISA*

567 IMCD3 cells were cultured in a 12-well culture plate and were pre-treated for 2 hours with either
568 Cyclopamine (10 μM) or Giripladib (GIRI, 4 μM) in serum free medium. Following pretreatment,
569 medium was changed to low serum containing either vehicle, Cyclopamine, or GIRI in control or
570 SHH-N conditioned media, and then incubated for 36 hours. PGE_2 levels were determined using
571 by ELISA (R&D Systems) according to the manufacturer's instructions. The absorbance of each
572 well was measured at 450 nm with correction at 540 nm.

573

574 *siRNA Transfection*

575 Transfections using Lipofectamine RNAiMAX were performed following the manufacturer's
576 protocols. Briefly, IMCD3 or NIH-3T3 cells were plated in a 6-well tissue culture plate at a
577 density of 175,000 or 100,000 cells per well. The following day, cells were treated with 25 pmol
578 of either the scrambled siRNA or *Adcy3, Adcy5*, *Adcy6* or *Ankmy2* siRNA. Cells were analyzed
579 48 hours post transfection.

580

581 *IFT88 Velocity*

582 To analyze intraciliary trafficking, Kymographs for anterograde IFT88 velocities were generated
583 in IMCD3 cells as previously described (Besschetnova et al., 2009). Briefly, 120,000 cells were
584 grown on a coverslip in a 24 well plate. Cells were transfected with IFT88-GFP and 5HT6-
585 mCherry plasmids the following day. Cells were pretreated with the EP4 inhibitor L161,982 for 2
586 hours and then switched to low serum media containing L161,982 either in the presence or
587 absence of SHH-N conditioned media and incubated overnight. On the day of the experiment,
588 the coverslips were flipped onto a 2-well chamber slide (Nunc™ Lab-Tek™ II Chamber Slide™
589 System) and the cells were imaged every 200 ms for 30 s on a Nikon A1R confocal microscope
590 with a 60x oil objective and 37 °C, 5% CO_2 heat stage (Live Cell Instrument). The resulting

591 videos were analyzed by ImageJ macros KymographClear and KymographDirect to generate
592 violin plots (Mangeol et al., 2016).

593

594 **QUANTIFICATION AND STATISTICAL ANALYSIS**

595 Quantification of ciliary lengths and SMO ciliary accumulation values were calculated from three
596 independent experiments with at least 100 cilia per condition per experiment. A maximum
597 fluorescence intensity projection from a sum of at least 10 slices was generated before length
598 and ciliary intensity quantifications. SMO ciliary intensity was normalized to acetylated α-tubulin
599 intensity. At least three randomly chosen fields of view were selected per condition per
600 experiment, and all cilia within the field were quantified using LAS X. For ciliary SMO signal
601 intensity determination, each cilium surface area was traced from the base to the tip using
602 spline profile function. The average fluorescence measurement adjacent to the cilium was
603 subtracted from ciliary fluorescence as background. The intensity values along the cilium were
604 exported and analyzed via GraphPad Prism. Colocalization of AC3 and AC6 within the primary
605 cilium marker ARL13B was carried out using the ImageJ plugin JACoP. Manders' coefficients
606 (M1 and M2) estimate the co-occurrence fraction of a fluorescent signal on one channel
607 (ARL13B) with a fluorescent signal of another channel (AC3/AC5/6). Manders' coefficients
608 range from 0 to 1. The former corresponds to non-overlapping images and the latter reflects a
609 complete co-localization between both images.

610

611 For quantification of cAMP, the red fluorescence and green fluorescence intensities over time
612 were processed on the Nikon NIS-Elements imaging software by defining a mask for each
613 cilium and determining the ratio of green fluorescence to red fluorescence. The data were

614 normalized to the initial time point for each experiment (set to 100%), and the inverse of each
615 value was plotted using GraphPad Prism.
616

617 Statistical analyses were performed using Prism 8 (GraphPad Software). Results are presented
618 as mean ± standard deviation. For comparisons between two groups, a two tailed unpaired t-
619 test was used unless otherwise specified. For multiple group comparisons, either one-way or
620 two-way (depending on the number of variables) ANOVA followed by multiple comparison post-
621 hoc testing was performed as indicated using Prism 8. Significance is depicted as *$p < 0.05$, **p
622 < 0.01, ***$p < 0.001$, ****$p < 0.0001$, ns = not significant.

623

624 **ACKNOWLEDGEMENTS**

625 We thank M. Hatley and members of the Ogden lab for reagents, advice, thoughtful discussion,
626 and comments on the manuscript. We thank S. Narumiya (Kyoto University) and the Center for
627 Animal Resources and Development (Kumamoto University) for providing *Ptger4*$^{-/-}$ frozen sperm
628 used to generate the *Ep*$_4^{-/-}$ mouse line. J. Reiter (UCSF) provided bPAC expression vectors, S.
629 Mukhopadhyay (UTSW) provided anti-GPR161, and M. Nachury (UCSF) provided Flp-In IMCD3
630 cells. We thank J. Temirov, J. Messing, A. Carisey, and the St. Jude CTIC for assistance with
631 confocal and electron microscopy. Diagrams were created with BioRender.com.

632

633 **FUNDING**

634 This work was supported by National Institute of Health grants R35GM122546 (S.K.O.) and
635 R01HD099777 (E.L.S.) and by ALSAC of St. Jude Children's Research Hospital. The CTIC is

supported by SJCRH and NCI P30 CA021765. The content is solely the responsibility of the authors and does not necessarily represent the official views of the funding agencies.

AUTHOR CONTRIBUTIONS

Conceptualization, S.S.A. and S.K.O.; Methodology, S.S.A., M.A.A., B.M.Y., M.E.D., Y.Z., E.L.S., A.J., C.G.R., and S.K.O.; Validation, S.S.A., M.A.A., M.E.D., and Y.Z.; Analysis, S.S.A., M.A.A., M.E.D., Y.Z., and A.J.; Investigation, S.S.A., M.A.A., M.E.D., and Y.Z.; Resources, J.D.S., Z.R., C.G.R., N.B., E.L.S., and S.K.O.; Writing – Original Draft, S.S.A. and S.K.O.; Writing – Review & Editing, S.S.A., M.E.D., J.D.S., E.L.S., and S.K.O.; Visualization, S.S.A.; Supervision, S.K.O. All authors approved the submitted manuscript.

DECLARATION OF INTERESTS

The authors declare no competing interests.

649 **REFERENCES**

650 Anvarian, Z., K. Mykytyn, S. Mukhopadhyay, L.B. Pedersen, and S.T. Christensen. 2019.
651 Cellular signalling by primary cilia in development, organ function and disease. *Nat Rev*
652 *Nephrol*. 15:199-219.
653 Arensdorf, A.M., M.E. Dillard, J.M. Menke, M.W. Frank, C.O. Rock, and S.K. Ogden. 2017.
654 Sonic Hedgehog Activates Phospholipase A2 to Enhance Smoothened Ciliary
655 Translocation. *Cell Rep*. 19:2074-2087.
656 Arensdorf, A.M., S. Marada, and S.K. Ogden. 2016. Smoothened Regulation: A Tale of Two
657 Signals. *Trends Pharmacol Sci*. 37:62-72.
658 Arveseth, C.D., J.T. Happ, D.S. Hedeen, J.F. Zhu, J.L. Capener, D. Klatt Shaw, I. Deshpande,
659 J. Liang, J. Xu, S.L. Stubben, I.B. Nelson, M.F. Walker, K. Kawakami, A. Inoue, N.J.
660 Krogan, D.J. Grunwald, R. Huttenhain, A. Manglik, and B.R. Myers. 2021. Smoothened
661 transduces Hedgehog signals via activity-dependent sequestration of PKA catalytic
662 subunits. *PLoS Biol*. 19:e3001191.
663 Bangs, F., and K.V. Anderson. 2017. Primary Cilia and Mammalian Hedgehog Signaling. *Cold*
664 *Spring Harb Perspect Biol*. 9.
665 Barakat, M.T., E.W. Humke, and M.P. Scott. 2010. Learning from Jekyll to control Hyde:
666 Hedgehog signaling in development and cancer. *Trends Mol Med*. 16:337-348.
667 Barzi, M., D. Kostrz, A. Menendez, and S. Pons. 2011. Sonic Hedgehog-induced proliferation
668 requires specific Galpha inhibitory proteins. *J Biol Chem*. 286:8067-8074.
669 Besschetnova, T.Y., E. Kolpakova-Hart, Y. Guan, J. Zhou, B.R. Olsen, and J.V. Shah. 2010.
670 Identification of signaling pathways regulating primary cilium length and flow-mediated
671 adaptation. *Curr Biol*. 20:182-187.
672 Besschetnova, T.Y., B. Roy, and J.V. Shah. 2009. Imaging intraflagellar transport in mammalian
673 primary cilia. *Methods Cell Biol*. 93:331-346.
674 Breslow, D.K., S. Hoogendoorn, A.R. Kopp, D.W. Morgens, B.K. Vu, M.C. Kennedy, K. Han, A.
675 Li, G.T. Hess, M.C. Bassik, J.K. Chen, and M.V. Nachury. 2018. A CRISPR-based
676 screen for Hedgehog signaling provides insights into ciliary function and ciliopathies. *Nat*
677 *Genet*. 50:460-471.
678 Breslow, D.K., and M.V. Nachury. 2015. Analysis of soluble protein entry into primary cilia using
679 semipermeabilized cells. *Methods Cell Biol*. 127:203-221.
680 Caspary, T., C.E. Larkins, and K.V. Anderson. 2007. The graded response to Sonic Hedgehog
681 depends on cilia architecture. *Dev Cell*. 12:767-778.
682 Cherukuri, D.P., X.B. Chen, A.C. Goulet, R.N. Young, Y. Han, R.L. Heimark, J.W. Regan, E.
683 Meuillet, and M.A. Nelson. 2007. The EP4 receptor antagonist, L-161,982, blocks
684 prostaglandin E2-induced signal transduction and cell proliferation in HCA-7 colon
685 cancer cells. *Exp Cell Res*. 313:2969-2979.
686 Duvernay, M.T., A. Matafonov, C.W. Lindsley, and H.E. Hamm. 2015. Platelet Lipidomic
687 Profiling: Novel Insight into Cytosolic Phospholipase A2alpha Activity and Its Role in
688 Human Platelet Activation. *Biochemistry*. 54:5578-5588.
689 Ericson, J., P. Rashbass, A. Schedl, S. Brenner-Morton, A. Kawakami, V. van Heyningen, T.M.
690 Jessell, and J. Briscoe. 1997. Pax6 controls progenitor cell identity and neuronal fate in
691 response to graded Shh signaling. *Cell*. 90:169-180.
692 Findakly, S., V. Daggubati, G. Garcia, S.A. LaStella, A. Choudhury, C. Tran, A. Li, P. Tong, J.Q.
693 Garcia, N. Puri, J.F. Reiter, L. Xu, and D.R. Raleigh. 2021. Sterol and oxysterol
694 synthases near the ciliary base activate the Hedgehog pathway. *J Cell Biol*. 220.
695 Garcia, G., 3rd, D.R. Raleigh, and J.F. Reiter. 2018. How the Ciliary Membrane Is Organized
696 Inside-Out to Communicate Outside-In. *Curr Biol*. 28:R421-R434.
697 Gayner, S.M., and T.V. McCaffrey. 1998. Muscarinic ciliostimulation requires endogenous
698 prostaglandin production. *Am J Rhinol*. 12:203-207.

699 Hansen, J.N., F. Kaiser, C. Klausen, B. Stuven, R. Chong, W. Bonigk, D.U. Mick, A. Moglich, N.
700 Jurisch-Yaksi, F.I. Schmidt, and D. Wachten. 2020. Nanobody-directed targeting of
701 optogenetic tools to study signaling in the primary cilium. *Elife*. 9.
702 Hansen, J.N., F. Kaiser, P. Leyendecker, B. Stuven, J.H. Krause, F. Derakhshandeh, J. Irfan,
703 T.J. Sroka, K.M. Preval, P.B. Desai, M. Kraut, H. Theis, A.D. Drews, E. De-Domenico, K.
704 Handler, G.J. Pazour, D.J.P. Henderson, D.U. Mick, and D. Wachten. 2022. A cAMP
705 signalosome in primary cilia drives gene expression and kidney cyst formation. *EMBO*
706 *Rep*. 23:e54315.
707 Happ, J.T., C.D. Arveseth, J. Bruystens, D. Bertinetti, I.B. Nelson, C. Olivieri, J. Zhang, D.S.
708 Hedeen, J.F. Zhu, J.L. Capener, J.W. Brockel, L. Vu, C.C. King, V.L. Ruiz-Perez, X. Ge,
709 G. Veglia, F.W. Herberg, S.S. Taylor, and B.R. Myers. 2022. A PKA inhibitor motif within
710 SMOOTHENED controls Hedgehog signal transduction. *Nat Struct Mol Biol*. 29:990-999.
711 Haxel, B.R., D. Schafer, L. Klimek, and W.J. Mann. 2001. Prostaglandin E2 activates the ciliary
712 beat frequency of cultured human nasal mucosa via the second messenger cyclic
713 adenosine monophosphate. *Eur Arch Otorhinolaryngol*. 258:230-235.
714 Haycraft, C.J., B. Banizs, Y. Aydin-Son, Q. Zhang, E.J. Michaud, and B.K. Yoder. 2005. Gli2
715 and Gli3 localize to cilia and require the intraflagellar transport protein polaris for
716 processing and function. *PLoS Genet*. 1:e53.
717 He, M., R. Subramanian, F. Bangs, T. Omelchenko, K.F. Liem, Jr., T.M. Kapoor, and K.V.
718 Anderson. 2014. The kinesin-4 protein Kif7 regulates mammalian Hedgehog signalling
719 by organizing the cilium tip compartment. *Nat Cell Biol*. 16:663-672.
720 Huangfu, D., and K.V. Anderson. 2006. Signaling from Smo to Ci/Gli: conservation and
721 divergence of Hedgehog pathways from Drosophila to vertebrates. *Development*. 133:3-
722 14.
723 Jia, J., C. Tong, B. Wang, L. Luo, and J. Jiang. 2004. Hedgehog signalling activity of
724 Smoothened requires phosphorylation by protein kinase A and casein kinase I. *Nature*.
725 432:1045-1050.
726 Jin, D., T.T. Ni, J. Sun, H. Wan, J.D. Amack, G. Yu, J. Fleming, C. Chiang, W. Li, A. Papierniak,
727 S. Cheepala, G. Conseil, S.P. Cole, B. Zhou, I.A. Drummond, J.D. Schuetz, J. Malicki,
728 and T.P. Zhong. 2014. Prostaglandin signalling regulates ciliogenesis by modulating
729 intraflagellar transport. *Nat Cell Biol*. 16:841-851.
730 Kinnebrew, M., E.J. Iverson, B.B. Patel, G.V. Pusapati, J.H. Kong, K.A. Johnson, G. Luchetti,
731 K.M. Eckert, J.G. McDonald, D.F. Covey, C. Siebold, A. Radhakrishnan, and R. Rohatgi.
732 2019. Cholesterol accessibility at the ciliary membrane controls hedgehog signaling.
733 *Elife*. 8.
734 Kinnebrew, M., G. Luchetti, R. Sircar, S. Frigui, L.V. Viti, T. Naito, F. Beckert, Y. Saheki, C.
735 Siebold, A. Radhakrishnan, and R. Rohatgi. 2021. Patched 1 reduces the accessibility of
736 cholesterol in the outer leaflet of membranes. *Elife*. 10.
737 Kong, J.H., C. Siebold, and R. Rohatgi. 2019. Biochemical mechanisms of vertebrate hedgehog
738 signaling. *Development*. 146.
739 Mangeol, P., B. Prevo, and E.J. Peterman. 2016. KymographClear and KymographDirect: two
740 tools for the automated quantitative analysis of molecular and cellular dynamics using
741 kymographs. *Mol Biol Cell*. 27:1948-1957.
742 Marra, A.N., B.D. Adeeb, B.E. Chambers, B.E. Drummond, M. Ulrich, A. Addiego, M. Springer,
743 S.J. Poureetezadi, J.M. Chambers, M. Ronshaugen, and R.A. Wingert. 2019.
744 Prostaglandin signaling regulates renal multiciliated cell specification and maturation.
745 *Proc Natl Acad Sci U S A*. 116:8409-8418.
746 May, E.A., M. Kalocsay, I.G. D'Auriac, P.S. Schuster, S.P. Gygi, M.V. Nachury, and D.U. Mick.
747 2021. Time-resolved proteomics profiling of the ciliary Hedgehog response. *J Cell Biol*.
748 220.

749 Mukhopadhyay, S., X. Wen, N. Ratti, A. Loktev, L. Rangell, S.J. Scales, and P.K. Jackson.
750 2013. The ciliary G-protein-coupled receptor Gpr161 negatively regulates the Sonic
751 hedgehog pathway via cAMP signaling. *Cell*. 152:210-223.
752 Niewiadomski, P., J.H. Kong, R. Ahrends, Y. Ma, E.W. Humke, S. Khan, M.N. Teruel, B.G.
753 Novitch, and R. Rohatgi. 2014. Gli protein activity is controlled by multisite
754 phosphorylation in vertebrate Hedgehog signaling. *Cell Rep*. 6:168-181.
755 Ogden, S.K., D.L. Fei, N.S. Schilling, Y.F. Ahmed, J. Hwa, and D.J. Robbins. 2008. G protein
756 Galphai functions immediately downstream of Smoothened in Hedgehog signalling.
757 *Nature*. 456:967-970.
758 Ott, C., and J. Lippincott-Schwartz. 2012. Visualization of live primary cilia dynamics using
759 fluorescence microscopy. *Curr Protoc Cell Biol*. Chapter 4:Unit 4 26.
760 Patten, I., and M. Placzek. 2000. The role of Sonic hedgehog in neural tube patterning. *Cell Mol*
761 *Life Sci*. 57:1695-1708.
762 Petrov, K., B.M. Wierbowski, and A. Salic. 2017. Sending and Receiving Hedgehog Signals.
763 *Annu Rev Cell Dev Biol*. 33:145-168.
764 Praktiknjo, S.D., F. Saad, D. Maier, P. Ip, and D.R. Hipfner. 2018. Activation of Smoothened in
765 the Hedgehog pathway unexpectedly increases Galphas-dependent cAMP levels in
766 Drosophila. *J Biol Chem*. 293:13496-13508.
767 Raleigh, D.R., N. Sever, P.K. Choksi, M.A. Sigg, K.M. Hines, B.M. Thompson, D. Elnatan, P.
768 Jaishankar, P. Bisignano, F.R. Garcia-Gonzalo, A.L. Krup, M. Eberl, E.F.X. Byrne, C.
769 Siebold, S.Y. Wong, A.R. Renslo, M. Grabe, J.G. McDonald, L. Xu, P.A. Beachy, and
770 J.F. Reiter. 2018. Cilia-Associated Oxysterols Activate Smoothened. *Mol Cell*. 72:316-
771 327 e315.
772 Ribes, V., and J. Briscoe. 2009. Establishing and interpreting graded Sonic Hedgehog signaling
773 during vertebrate neural tube patterning: the role of negative feedback. *Cold Spring Harb*
774 *Perspect Biol*. 1:a002014.
775 Riobo, N.A., and D.R. Manning. 2007. Pathways of signal transduction employed by vertebrate
776 Hedgehogs. *Biochem J*. 403:369-379.
777 Segi, E., Y. Sugimoto, A. Yamasaki, Y. Aze, H. Oida, T. Nishimura, T. Murata, T. Matsuoka, F.
778 Ushikubi, M. Hirose, T. Tanaka, N. Yoshida, S. Narumiya, and A. Ichikawa. 1998. Patent
779 ductus arteriosus and neonatal death in prostaglandin receptor EP4-deficient mice.
780 *Biochem Biophys Res Commun*. 246:7-12.
781 Shi, X., G. Garcia, 3rd, J.C. Van De Weghe, R. McGorty, G.J. Pazour, D. Doherty, B. Huang,
782 and J.F. Reiter. 2017. Super-resolution microscopy reveals that disruption of ciliary
783 transition-zone architecture causes Joubert syndrome. *Nat Cell Biol*. 19:1178-1188.
784 Somatilaka, B.N., S.H. Hwang, V.R. Palicharla, K.A. White, H. Badgandi, J.M. Shelton, and S.
785 Mukhopadhyay. 2020. Ankmy2 Prevents Smoothened-Independent Hyperactivation of
786 the Hedgehog Pathway via Cilia-Regulated Adenylyl Cyclase Signaling. *Dev Cell*.
787 54:710-726 e718.
788 Thotala, D., J.M. Craft, D.J. Ferraro, R.P. Kotipatruni, S.R. Bhave, J.J. Jaboin, and D.E.
789 Hallahan. 2013. Cytosolic phospholipaseA2 inhibition with PLA-695 radiosensitizes
790 tumors in lung cancer animal models. *PLoS One*. 8:e69688.
791 Truong, M.E., S. Bilekova, S.P. Choksi, W. Li, L.J. Bugaj, K. Xu, and J.F. Reiter. 2021.
792 Vertebrate cells differentially interpret ciliary and extraciliary cAMP. *Cell*. 184:2911-2926
793 e2918.
794 Tuson, M., M. He, and K.V. Anderson. 2011. Protein kinase A acts at the basal body of the
795 primary cilium to prevent Gli2 activation and ventralization of the mouse neural tube.
796 *Development*. 138:4921-4930.
797 Umberger, P.A., and S.K. Ogden. 2021. SPOP and CUL3 Modulate the Sonic Hedgehog Signal
798 Response Through Controlled Degradation of GLI Family Transcription Factors. *Front*
799 *Cell Dev Biol*. 9:710295.

800 Vuolo, L., A. Herrera, B. Torroba, A. Menendez, and S. Pons. 2015. Ciliary adenylyl cyclases
801 control the Hedgehog pathway. *J Cell Sci*. 128:2928-2937.
802 Wheway, G., L. Nazlamova, and J.T. Hancock. 2018. Signaling through the Primary Cilium.
803 *Front Cell Dev Biol*. 6:8.
804 Wijaya, J., B.T. Vo, J. Liu, B. Xu, G. Wu, Y. Wang, J. Peng, J. Zhang, L.J. Janke, B.A. Orr, J.
805 Yu, M.F. Roussel, and J.D. Schuetz. 2020. An ABC Transporter Drives Medulloblastoma
806 Pathogenesis by Regulating Sonic Hedgehog Signaling. *Cancer Res*. 80:1524-1537.
807 Ye, F., D.K. Breslow, E.F. Koslover, A.J. Spakowitz, W.J. Nelson, and M.V. Nachury. 2013.
808 Single molecule imaging reveals a major role for diffusion in the exploration of ciliary
809 space by signaling receptors. *Elife*. 2:e00654.
810 Zhang, P., B. Fan, P. Yang, J. Temirov, J. Messing, H.J. Kim, and J.P. Taylor. 2019. Chronic
811 optogenetic induction of stress granules is cytotoxic and reveals the evolution of ALS-
812 FTD pathology. *Elife*. 8.
813 Zhou, X., L.X. Fan, K. Li, R. Ramchandran, J.P. Calvet, and X. Li. 2014. SIRT2 regulates
814 ciliogenesis and contributes to abnormal centrosome amplification caused by loss of
815 polycystin-1. *Hum Mol Genet*. 23:1644-1655.

816

817 **FIGURE LEGENDS**

818 **Figure 1: PGE_2 generated downstream of SHH contributes to ciliary length control. (A-A')**.
819 PGE_2 is secreted downstream of SMO and $cPLA_2$ activation. PGE_2 was measured in IMCD3 **(A)**
820 or WT and *Abcc4*$^{-/-}$ NIH-3T3 **(A')** cell culture media by ELISA. **(A).** Cells were pretreated with
821 vehicle control (DMSO), the inverse SMO agonist cyclopamine (10 μM), or $cPLA_2$ inhibitor
822 giripladib (GIRI, 2 μM), and then exposed to SHH. PGE_2 was measured in cell culture
823 supernatant ~36 hours post treatment. The experiment was repeated twice with 3 biological
824 replicates per experiment. Pooled data are shown. **(A').** Cells were pretreated with vehicle
825 (DMSO), cyclopamine (10 μM), or COX2 inhibitor Celecoxib (Coxib,10 μM) and then stimulated
826 with control or SHH conditioned media. PGE_2 was measured in the supernatant ~36 hours after
827 treatment. The experiment was performed twice with 3 biological replicates per experiment. A
828 representative experiment is shown. **(B-C).** $cPLA_2$ inhibition shortens primary cilia. **(B)**. IMCD3
829 cells were treated with SHH conditioned media in the presence of GIRI (4 μM), or vehicle control
830 (DMSO). The ciliary axoneme is marked by acetylated α-tubulin (magenta). DAPI (blue) marks
831 the nucleus. Scale bar = 10 μm. **(C)**. Lengths of primary cilia were quantified in IMCD3 cells
832 treated with SHH conditioned media in the absence or presence of GIRI. Average primary cilium
833 length was determined by measuring cilia of ≥100 cells/condition across three independent
834 experiments. **(D-E).** PGE_2 supplementation rescues ciliary length in GIRI-treated IMCD3 cells.
835 Cells were treated with 4 μM GIRI in the presence of PGE_2 media supplementation (40 μM) or
836 vehicle control. Scale bar = 10 μm. Ciliary length quantification is shown in **E. (F-G).** Arachidonic
837 acid supplementation rescues primary cilium length following $cPLA_2$ inhibition. IMCD3 cells were
838 treated with SHH conditioned media in the presence of vehicle or 4 μM GIRI in media
839 supplemented with increasing concentrations of arachidonic acid (12.5 μM or 25 μM). Scale bar
840 = 10 μm. Ciliary length quantification is shown in **G**. For all experiments, statistical significance
841 was calculated using one-way ANOVA. A p value of less than 0.05 was considered statistically

842 significant with significance indicated as follows: *<0.05, **<0.01, ***<0.001, ****<0.0001, and
843 ns, p > 0.05. Data are represented as mean ± SD.

844

845 **Figure 2: EP_4 is required for primary cilium length homeostasis. (A).** EP_4 localizes to
846 primary cilia of IMCD3 cells. Endogenous EP_4 is shown in green and acetylated α-tubulin
847 (magenta) marks the primary cilium. Scale bar = 5 μm. **(B-C').** EP_4 localizes to primary cilia in
848 wild type MEFs. Ciliary EP_4 signal is absent in *$Ep_4^{-/-}$* cells. Line scans indicate the degree of
849 localization between EP_4 (green) and acetylated α-tubulin (magenta) within the primary cilium in
850 control **(B')** and *$Ep_4^{-/-}$* MEFs **(C')**. Intensity profiles are presented as arbitrary units (AU). Scale
851 bars = 5 μm. **(D).** EP_4 inhibition shortens primary cilia in IMCD3 cells. Cells were pretreated with
852 vehicle control (DMSO) or EP_4 inhibitor L161,982 (10 μM or 20 μM) for two hours prior to
853 addition of SHH. **(E).** PGE_2 partially rescues primary cilia length following EP_4 inhibition. IMCD3
854 cells were treated with SHH conditioned media in the presence of vehicle or 20 μM L161,982 in
855 media supplemented with increasing concentrations of PGE_2 (25 or 50 μM). At least 150
856 cilia/condition were measured over three experiments. Statistical significance was calculated
857 using one-way ANOVA. For all experiments, a p value of less than 0.05 was considered
858 statistically significant with significance indicated as follows: *<0.05, **<0.01, ***<0.001,
859 ****<0.0001, and ns, p > 0.05. Data are represented as mean ± SD.

860

861 **Figure 3: SHH signaling is attenuated by inhibition of $cPLA_2$ or EP_4. (A-B).** SMO ciliary
862 enrichment is reduced by EP_4 inhibition. SMO (**A,** red) enrichment in primary cilia was examined
863 in IMCD3 cells. Primary cilia are marked with acetylated α-tubulin (magenta). Cells were
864 pretreated with vehicle (DMSO), GIRI (4 μM), or L161,982 (20 μM) for 18 hours. Scale bar = 5
865 μm. **(B).** Average SMO ciliary signal intensity was quantified for each condition. **(C-E).** EP_4 loss

866 shortens primary cilia and attenuates SMO ciliary enrichment. Ciliary length and SMO (red)
867 ciliary enrichment were examined in wild type and *Ep4*$^{-/-}$ MEFs 18 hours post treatment with
868 control or SHH conditioned media. Cilia are marked by acetylated α-tubulin (magenta, **C**). Scale
869 bar =10 μm. A representative experiment is shown. Quantification of average primary cilium
870 length **(D)** and ciliary SMO signal intensity **(E)** were determined as above by measuring cilia of
871 ≥150 cells/condition across three independent experiments. **(F-F').** qRT-PCR analyses of *Gli1*
872 and *Ptch1* expression in IMCD3 and NIH-3T3 cells were performed. Cells were pretreated with
873 vehicle (DMSO), GIRI (4 μM), or L161,982 (10 μM) for 2 hours and then cultured in control or
874 SHH conditioned media plus inhibitor for 18 hours. Fold-change in expression was determined
875 using the $2^{-\Delta\Delta Ct}$ method. Average fold change was calculated across two independent
876 experiments with three biological replicates per experiment. All data are pooled. For all
877 experiments, statistical significance was determined using a one-way ANOVA. A p value of less
878 than 0.05 was considered statistically significant. Significance is denoted as follows: *<0.05,
879 **<0.01, ***<0.001, ****<0.0001, and ns, p > 0.05. Error bars indicate SD.

880

881 **Figure 4: Ciliary adenylyl cyclases contribute to primary cilium length control and SHH-**
882 **stimulated transcriptional activation. (A).** A model for SHH and EP_4 effects on primary cilium
883 cAMP control. **(B-D).** Knockdown of ciliary AC3, AC5, or AC6 disrupts ciliary cAMP control,
884 shortens primary cilia, and compromises *Gli1* induction. **(B).** IMCD3 cells were treated with
885 scrambled, *Adcy3*, *Adcy5,* or *Adcy6* siRNA for 48 hours and ciliary cAMP was measured using
886 the cADDis cAMP sensor. cADDis activity was recorded as cells were exposed to vehicle
887 (ethanol, black) or forskolin (FSK,100 μM, blue). Fluorescence ciliary intensity was recorded
888 over 8 minutes in live cell imaging mode. An average of ~5 cilia were recorded for each
889 condition. The experiment was performed three times. A representative experiment is shown.
890 Significance was determined by calculating the area under the curve followed by Student's t-test

891 analysis. **(C)**. Ciliary AC knockdown shortens primary cilia. Knockdown experiments were
892 repeated at least twice with 75-100 primary cilia measured per experiment per condition. All
893 data were pooled. Significance was determined by one-way ANOVA. **(D)**. *Gli1* fold change was
894 determined in control and SHH-stimulated IMCD3 cells following *Adcy3*, *Adcy5*, or *Adcy6*
895 knockdown. Fold change was assessed by qRT-PCR ~48 hours after treatment with AC-specific
896 siRNA or scrambled control following 2 hours of serum starvation and overnight treatment with
897 SHH conditioned media. Expression was determined using the $2^{-\Delta\Delta Ct}$ method. Significance was
898 determined by a one-way ANOVA. **(E-F)**. Knockdown of *Ankmy2* shortens primary cilia and
899 attenuates ligand-stimulated *Gli1* induction. **(E).** Knockdown experiments were repeated at least
900 twice with 75-100 primary cilia measured per experiment per condition. All data were pooled.
901 Significance was determined by Student's t-test **(F).** *Gli1* fold change was determined in control
902 or SHH-stimulated IMCD3 cells following *Ankmy2* knockdown, as described above. The
903 experiment was performed twice in triplicate and all data pooled. Significance was determined
904 by a one-way ANOVA. For all experiments, a p value of less than 0.05 was considered
905 statistically significant. Significance is denoted as follows: *<0.05, **<0.01, ***<0.001,
906 ****<0.0001, and ns, p > 0.05. Error bars indicate SD.

907

908 **Figure 5: EP_4 stabilizes ciliary cAMP in SHH-stimulated cells to maintain anterograde IFT**
909 **and SMO ciliary accumulation. (A).** EP_4 signaling equilibrates SMO-induced reduction of
910 primary cilium cAMP. cADDis-expressing IMCD3 cells were pretreated overnight with vehicle or
911 L161,982 (10 μM). The following morning, cADDis activity was monitored by live imaging to
912 track the ciliary cAMP response as cells were treated with forskolin (FSK, 100 μM) for 1.5
913 minutes prior to addition of the SMO agonist SAG (1 μM) or vehicle control. Fluorescence ciliary
914 intensity was recorded over 10 minutes in live cell imaging mode. An average of ~6 cilia were
915 recorded for each condition and the experiment was performed twice. A representative

916 experiment is shown. **(B)**. Anterograde IFT velocity was calculated in IMCD3 cells by tracking
917 IFT88-GFP movement in the presence and absence of SHH, L161,982 (10 μM), or vehicle
918 control. IFT velocity was calculated for 30 cilia per condition across 4 experiments. Velocity is
919 shown as a violin plot with SD indicated. **(C-D).** Average ciliary length and SMO ciliary intensity
920 were quantified in IMCD3-bPAC cells exposed to control or SHH conditioned media in the
921 absence or presence of 10 μM L161,982 in control or blue light-exposed cells. Significance was
922 determined by one-way ANOVA. For all experiments, a p value of less than 0.05 was
923 considered statistically significant. Significance is denoted as follows: *<0.05, **<0.01,
924 ***<0.001, ****<0.0001, and ns, p > 0.05. Data are represented as mean ± SD. For all ciliary
925 analyses, 50-100 cells per condition were analyzed over at least 3 independent experiments.

926

927 **Figure 6: EP_4 loss *in vivo* reduces primary cilium length and alters SHH-dependent neural**
928 **tube patterning. (A)**. Scanning electron microscopy images of cardiac level neural tube
929 sections from E9.5/27 somite stage *Ep4*$^{+/-}$ and *Ep4*$^{-/-}$ embryos show apical plasma membranes
930 of cells lining the neural tube lumen. Scale bar = 2 μm. Cilia are shaded in pink **(B)**. Average
931 primary cilium length was calculated by measuring cilia of ~30 cells/embryo lining the neural
932 tube lumen. Primary cilia of *Ep*$_4^{-/-}$ embryos show a statistically significant length reduction.
933 Statistical significance was calculated using one-way ANOVA. Error bars indicate SD**.**
934 Significance is denoted as follows: ****<0.0001, and ns, p > 0.05. **(C-D).** *Ep*$_4^{-/-}$ embryos show
935 altered ventral progenitor domains. Cardiac level sections of E9.5/29 somite stage neural tubes
936 from the indicated genotypes were immuno-stained for neural progenitor domain markers *Olig2*
937 (magenta) and *Pax6* (green). *Ep*$_4^{-/-}$ neural tubes show disrupted ventral progenitor specification
938 as indicated by reduced *Olig2*-labeled cellular populations. For all experiments, four embryos
939 per genotype were analyzed. Scale bar = 100 μm. Progenitor domain area is shown in **(D)**.
940 Statistical significance was calculated using a Student's t-test. Error bars indicate SD**.**

941 Significance is denoted as follows: *<0.05. Sections shown in **(C)** are indicated as colored dots
942 in each graph.

943

944 **Figure 7: A model for SHH-to-EP4 signal crosstalk. (A).** In the absence of SHH, the SHH
945 receptor PTCH prevents ciliary accumulation and signaling of the GPCR SMO. In this basal
946 condition, GPR161 signaling and basal PGE_2 secretion and activation of EP_4-$G\alpha_s$ maintain
947 sufficient ciliary cAMP for anterograde IFT and length homeostasis. **(B).** SHH binding to PTCH
948 leads to SMO de-repression and GPR161 ciliary exit. SMO activates $G\alpha_i\beta\gamma$ to increase
949 production of arachidonic acid by βγ stimulation of $cPLA_2\alpha$. Arachidonic acid is metabolized to
950 PGE_2, which is secreted to activate ciliary EP_4 for $G\alpha_s$ activation. This ensures ciliary cAMP
951 levels remain sufficiently high in SHH-stimulated cells to prevent anterograde IFT slowing that
952 leads ciliary shortening. **(C).** Inhibition of $cPLA_2$ or EP_4 reduces SHH-to-EP_4 signal crosstalk,
953 reduces primary cilium length, and blunts SMO ciliary accumulation and high-level signaling.

954

955 **SUPPLEMENTARY FIGURE LEGENDS**

956 **Supplementary Figure 1: $cPLA_2$ is required for SMO ciliary accumulation but not for**
957 **GPR161 ciliary exit. (A-D).** IMCD3 cells were treated with vehicle **(A-B)** or GIRI **(C-D**, 4 μM**)** in
958 the absence or presence of SHH as indicated. GPR161 is magenta, SMO is red, ARL13B
959 (green) marks primary cilia. Scale bar = 3 μm. **(E-E')**. Quantification of ciliary signal intensity for
960 SMO **(E)** and GPR161 **(E')** in cells treated with SHH, GIRI, or vehicle control. The experiment
961 was performed twice with at least 30 cilia imaged per condition per experiment and all data were
962 pooled. Significance was determined using a one-way ANOVA. Significance is indicated as
963 follows: *<0.05, **<0.01, ***<0.001, ****<0.0001, and ns, p > 0.05.

964

965 **Supplementary Figure 2: Ciliary AC controls primary cilium cAMP. (A).** AC3 and AC5/6
966 localize to primary cilia in IMCD3 cells. ARL13B (magenta in merge and white in insets) marks
967 primary cilia. Ciliary ACs are shown in green (merge) and in white (insets). Scale bar = 5μm.
968 **(B).** *Adcy3*, *Adcy5,* or *Adcy6* knockdown in IMCD3 cells was validated by qRT-PCR ~48 hours
969 after treatment with AC-specific siRNA or scrambled control. Fold-change in expression was
970 determined using the $2^{-\Delta\Delta Ct}$ method. Experiments were performed 3 times in triplicate and all
971 data pooled. Statistical significance was calculated using Student's t-test. **(C).** Knockdown of
972 ciliary AC does not alter forskolin (FSK)-stimulated whole cell cAMP elevation. The indicated
973 ciliary AC were knocked down as above. Cells were stimulated with 100 μM forskolin ~48 hours
974 after siRNA treatment and whole cell cAMP was measured using the direct cAMP ELISA assay.
975 Assays were performed at least 3 times and all data pooled. Statistical significance was
976 calculated using Student's t-test. **(D-F')**. Live imaging of cADDis-expressing IMCD3 cells shows
977 changes in fluorescence intensity of a ciliary cAMP sensor (green) and stable fluorescence of
978 the ciliary reference marker (magenta) following exposure to vehicle **(D)** or forskolin (FSK, 100
979 μM) **(E)**. Increasing cAMP decreases green fluorescence. Scale bar = 2 μm. **(F-F').** Relative

980 cAMP shift is shown as native **(F)** or inverse **(F')** of the fluorescent intensity ratio of the cAMP
981 sensor to reference marker. Inverse ratios are shown in the main figures to clearly illustrate
982 cAMP increase. Significance was determined by calculating the area under the curve followed
983 by Student's t-test analysis. Significance is indicated as follows: *<0.05, **<0.01, ***<0.001,
984 ****<0.0001, and ns, p > 0.05.

985 **Supplementary Figure 3: *Ankmy2* knockdown impacts IMCD3 ciliary AC enrichment and**
986 **SHH-stimulated transcriptional activation. (A).** qRT-PCR verification of *Ankmy2* knockdown
987 in IMCD3 cells ~48 hours after treatment with *Ankmy2* siRNA or scrambled control. Fold-change
988 in expression was determined using the $2^{-\Delta\Delta Ct}$ method. **(B-C)**. Knockdown of the ciliary AC
989 chaperone *Ankmy2* reduces primary cilium AC occupancy. Colocalization of AC3 **(B)** and AC5/6
990 **(C)** to ARL13B in primary cilia of IMCD3 cells in scrambled and *Ankmy2* siRNA-treated cells is
991 shown. Both M1 and M2 scores of AC3 and AC5/6 to ARL13B are significantly reduced in cilia
992 of the *Ankmy2* siRNA treated cells compared to control. Statistical significance was calculated
993 using Student's t-test. **(D)**. *Ankmy2* knockdown reduces forskolin-induced ciliary cAMP increase.
994 Forskolin (FSK) induced changes in primary cilium cAMP were monitored in *Ankmy2*
995 knockdown cells using the CADDis sensor. Forskolin-mediated ciliary cAMP accumulation is
996 blocked by *Ankmy2* knockdown. Significance was determined by calculating the area under the
997 curve followed by Student's t-test analysis. **(E)**. *Adcy3*, *Adcy5,* and *Anmky2* knockdown in NIH-
998 3T3 cells was validated by qRT-PCR ~48 hours after treatment with *Adcy3, Adcy5,* or *Ankmy2*
999 siRNA or scrambled control. Fold-change in expression was determined using the $2^{-\Delta\Delta Ct}$
1000 method. Student's t-test was used to calculate statistical significance. **(F-G)**. Knockdown of
1001 *Adcy3, Adcy5,* or *Ankmy2* shortens primary cilia and reduces SHH target gene induction in NIH-
1002 3T3 cells. **(F)**. Average lengths of ARL13B marked primary cilia of NIH-3T3 cells were
1003 determined as described above. Knockdown experiments were repeated three times with 75-
1004 100 primary cilia measured per condition per experiment. **(G)**. *Gli1* fold change was determined

1005 in control or SHH-stimulated NIH-3T3 cells following *Adcy3, Adcy5,* or *Ankmy2* knockdown.
1006 Significance was determined by one-way ANOVA. For all experiments, significance is denoted
1007 as follows: *<0.05, **<0.01, ***<0.001, ****<0.0001, and ns, p > 0.05. Data are represented as
1008 mean ± SD. qPCR analyses were performed twice in triplicate and all data were pooled.

1009

1010 **Supplementary Figure 4: Validation of optogenetic cAMP modulation in IMCD3 cells. (A).**
1011 Schematic of optogenetic cAMP modulation. Ciliary bPAC is activated by blue light to increase
1012 ciliary cAMP**. (B).** Immunofluorescence imaging of IMCD3 cells expressing Cyto-bPAC-GFP or
1013 Cilia-bPAC-GFP (green). Acetylated α-tubulin marks cilia (magenta) and DAPI (blue) marks
1014 nuclei. Scale bars = 10 μm. **(C-C").** Average ciliary length was quantified in IMCD3 Cyto-bPAC,
1015 and IMCD3 Cilia-bPAC cells in control conditions or following 180 minutes of blue light
1016 exposure. **(C').** Total cellular cAMP was measured as in Supplementary Figure 2C. Error bars
1017 indicate SD. Significance was determined by a one-way ANOVA in **(C)** and a Student's t-test in
1018 **(C')**. **(D-D').** Ciliary lengths were measured in vehicle and forskolin treated cells. Average
1019 primary cilium length was calculated by measuring cilia of ≥100 cells/condition across three
1020 independent experiments. All data were pooled. **(D').** IMCD3 cells were treated with vehicle or
1021 100 μM forskolin. The ciliary axoneme is marked by ARL13B (magenta) and DAPI (blue) marks
1022 nuclei. Scale bar = 5 μm. Significance was determined using a one-way ANOVA. For all
1023 experiments significance is indicated as follows: *<0.05, **<0.01, ***<0.001, ****<0.0001, and
1024 ns, p > 0.05.

Figure 1

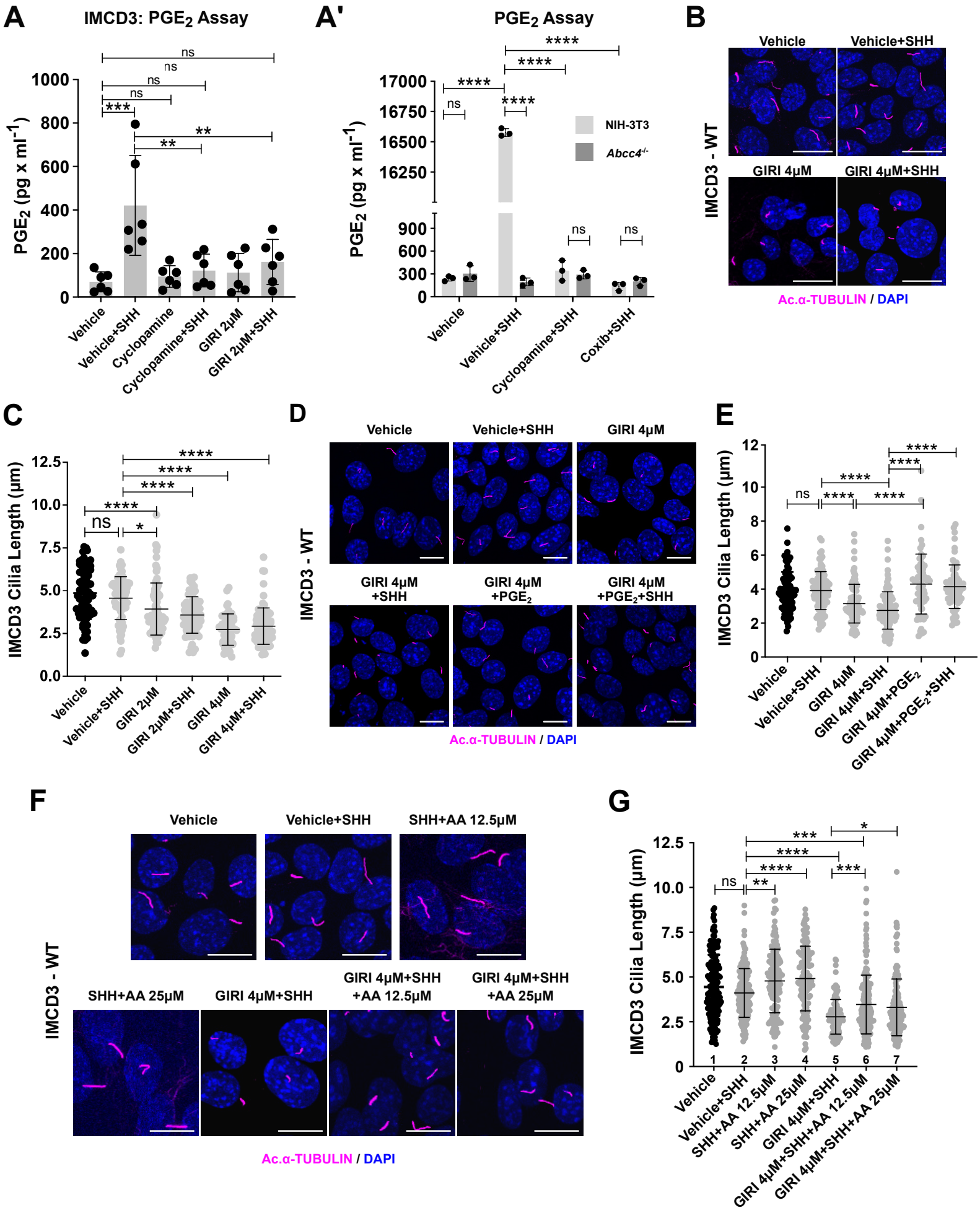
A
IMCD3: PGE2 Assay
PGE2 (pg x ml-1)
1000
800
600
400
200
0
ns
ns
ns
ns
***
**
**
Vehicle
Vehicle+SHH
Cyclopamine
Cyclopamine+SHH
GIRI 2μM
GIRI 2μM+SHH
A'
PGE2 Assay
PGE2 (pg x ml-1)
17000
16750
16500
16250
900
600
300
0
****
****
****
ns
****
NIH-3T3
Abcc4-/-
ns
ns
Vehicle
Vehicle+SHH
Cyclopamine+SHH
Coxib+SHH
B
Vehicle
Vehicle+SHH
GIRI 4μM
GIRI 4μM+SHH
IMCD3 - WT
Ac.α-TUBULIN / DAPI
C
IMCD3 Cilia Length (μm)
12.5
10.0
7.5
5.0
2.5
0.0
****
****
****
****
ns
*
Vehicle
Vehicle+SHH
GIRI 2μM
GIRI 2μM+SHH
GIRI 4μM
GIRI 4μM+SHH
D
Vehicle
Vehicle+SHH
GIRI 4μM
GIRI 4μM +SHH
GIRI 4μM +PGE2
GIRI 4μM +PGE2+SHH
IMCD3 - WT
Ac.α-TUBULIN / DAPI
E
IMCD3 Cilia Length (μm)
12
10
8
6
4
2
0
****
****
****
ns
****
****
Vehicle
Vehicle+SHH
GIRI 4μM
GIRI 4μM+SHH
GIRI 4μM+PGE2
GIRI 4μM+PGE2+SHH
F
Vehicle
Vehicle+SHH
SHH+AA 12.5μM
SHH+AA 25μM
GIRI 4μM+SHH
GIRI 4μM+SHH +AA 12.5μM
GIRI 4μM+SHH +AA 25μM
IMCD3 - WT
Ac.α-TUBULIN / DAPI
G
IMCD3 Cilia Length (μm)
12.5
10.0
7.5
5.0
2.5
0
***
*
****
****
***
ns
**
1
2
3
4
5
6
7
Vehicle
Vehicle+SHH
SHH+AA 12.5μM
SHH+AA 25μM
GIRI 4μM+SHH
GIRI 4μM+SHH+AA 12.5μM
GIRI 4μM+SHH+AA 25μM

Figure 2

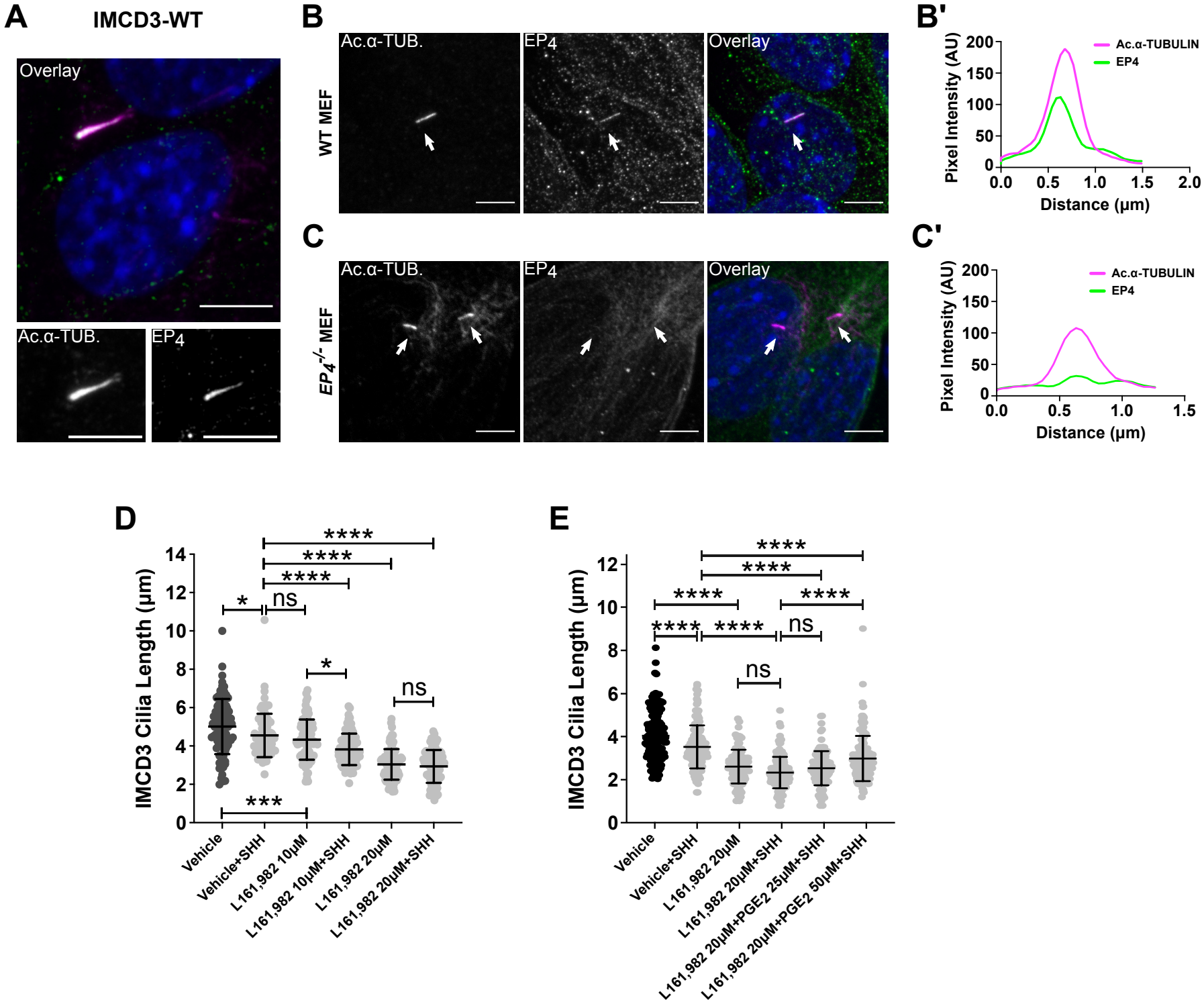
A
IMCD3-WT
Overlay
Ac.α-TUB.
EP4
B
WT MEF
Ac.α-TUB.
EP4
Overlay
B'
Ac.α-TUBULIN
EP4
Pixel Intensity (AU)
Distance (μm)
C
EP4-/- MEF
Ac.α-TUB.
EP4
Overlay
C'
Ac.α-TUBULIN
EP4
Pixel Intensity (AU)
Distance (μm)
D
IMCD3 Cilia Length (μm)
Vehicle
Vehicle+SHH
L161,982 10μM
L161,982 10μM+SHH
L161,982 20μM
L161,982 20μM+SHH
E
IMCD3 Cilia Length (μm)
Vehicle
Vehicle+SHH
L161,982 20μM
L161,982 20μM+SHH
L161,982 20μM+PGE2 25μM+SHH
L161,982 20μM+PGE2 50μM+SHH

Figure 3

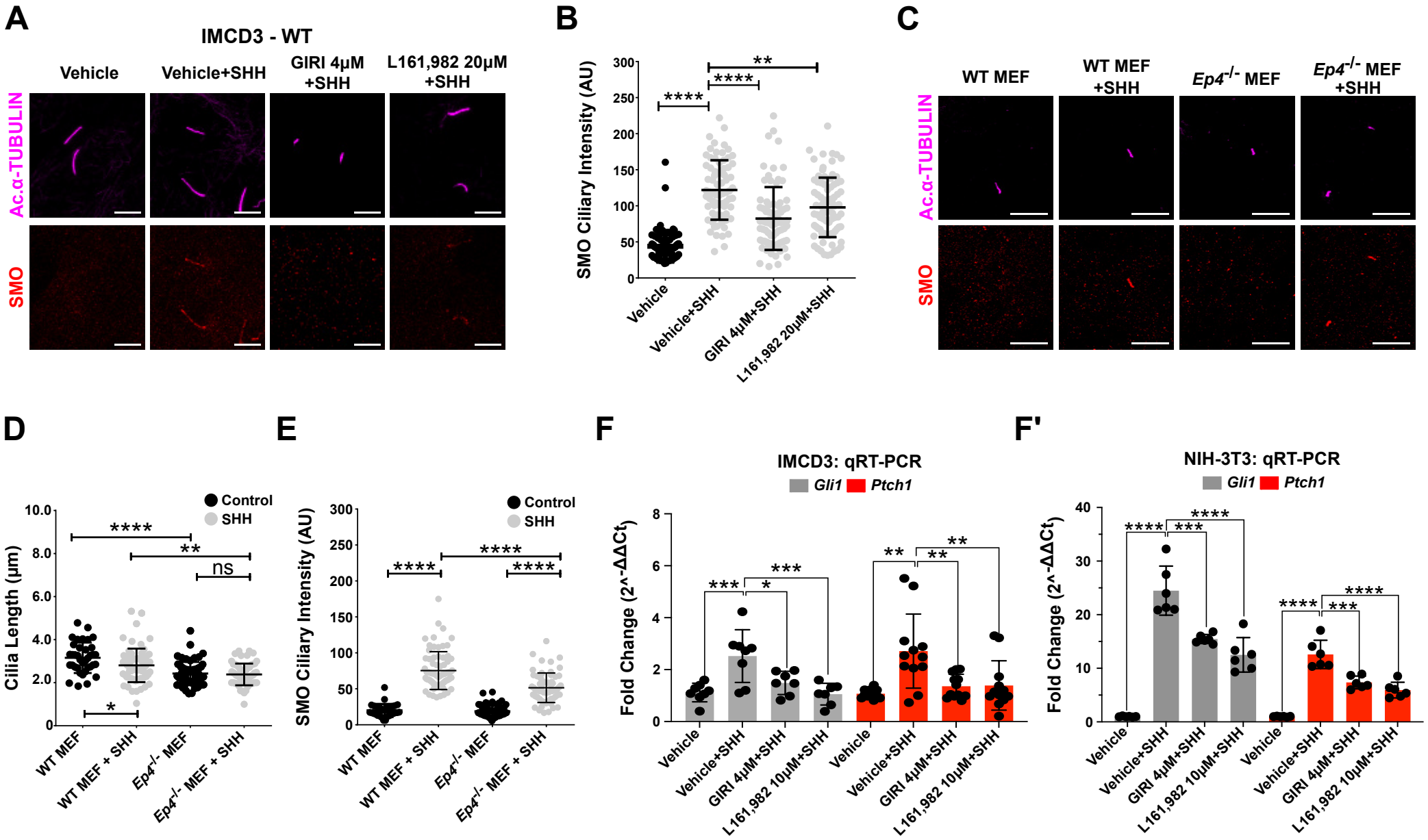
A
IMCD3 - WT
Vehicle
Vehicle+SHH
GIRI 4μM +SHH
L161,982 20μM +SHH
Ac.α-TUBULIN
SMO
B
SMO Ciliary Intensity (AU)
Vehicle
Vehicle+SHH
GIRI 4μM+SHH
L161,982 20μM+SHH
C
WT MEF
WT MEF +SHH
Ep4-/- MEF
Ep4-/- MEF +SHH
D
Cilia Length (μm)
Control
SHH
ns
WT MEF
WT MEF + SHH
Ep4-/- MEF
Ep4-/- MEF + SHH
E
SMO Ciliary Intensity (AU)
F
IMCD3: qRT-PCR
Gli1
Ptch1
Fold Change (2^-ΔΔCt)
Vehicle
Vehicle+SHH
GIRI 4μM+SHH
L161,982 10μM+SHH
F'
NIH-3T3: qRT-PCR

Figure 4

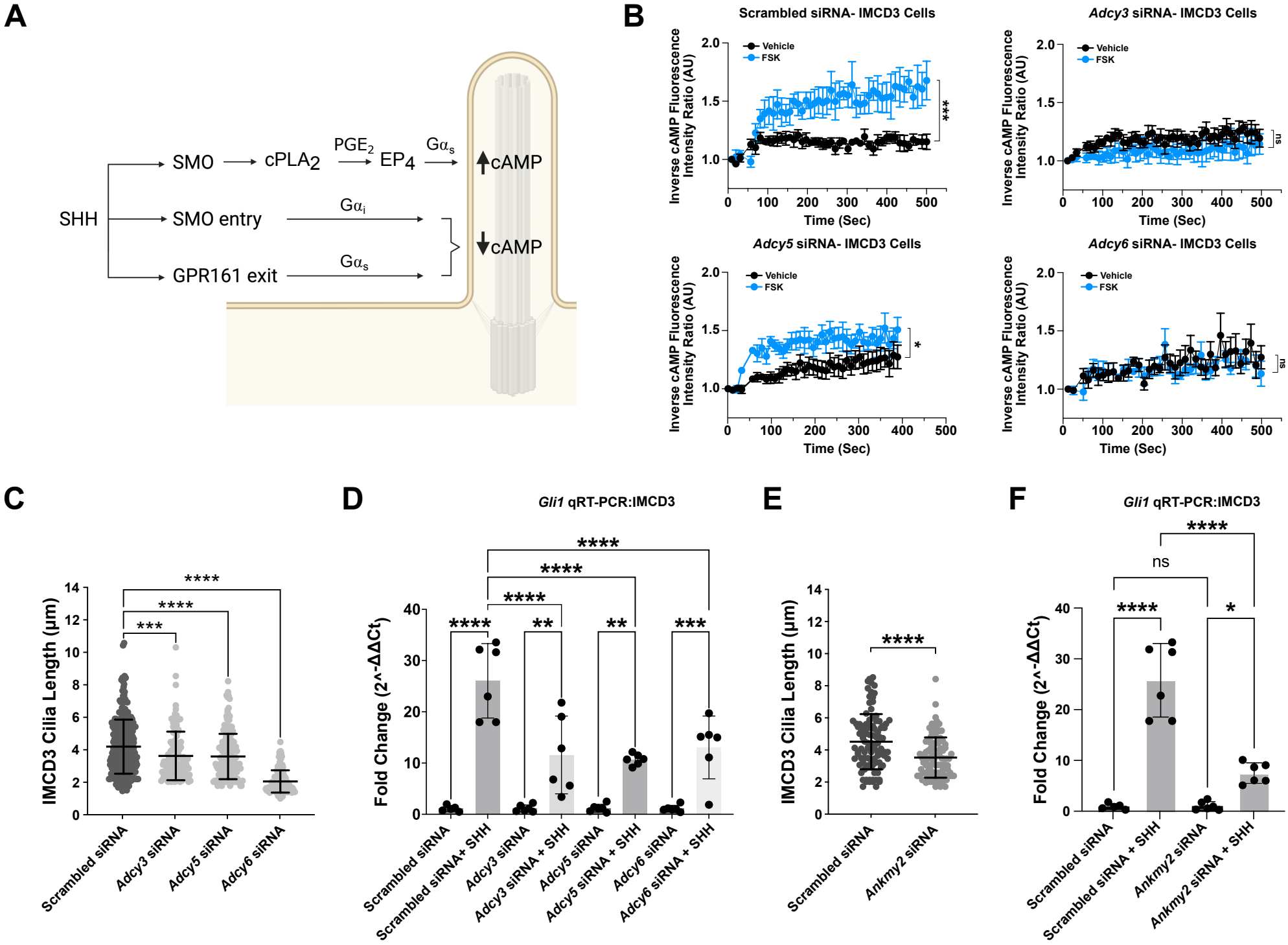
A
SHH
SMO
cPLA2
PGE2
EP4
Gαs
cAMP
SMO entry
Gαi
GPR161 exit
Gαs
cAMP
B
Scrambled siRNA- IMCD3 Cells
Adcy3 siRNA- IMCD3 Cells
Adcy5 siRNA- IMCD3 Cells
Adcy6 siRNA- IMCD3 Cells
Vehicle
FSK
Inverse cAMP Fluorescence Intensity Ratio (AU)
Time (Sec)
***
ns
*
ns
C
IMCD3 Cilia Length (µm)
Scrambled siRNA
Adcy3 siRNA
Adcy5 siRNA
Adcy6 siRNA
D
Gli1 qRT-PCR:IMCD3
Fold Change (2^-ΔΔCt)
Scrambled siRNA
Scrambled siRNA+ SHH
Adcy3 siRNA
Adcy3 siRNA + SHH
Adcy5 siRNA
Adcy5 siRNA + SHH
Adcy6 siRNA
Adcy6 siRNA + SHH
E
IMCD3 Cilia Length (µm)
Scrambled siRNA
Ankmy2 siRNA
F
Gli1 qRT-PCR:IMCD3
Fold Change (2^-ΔΔCt)
ns
Scrambled siRNA
Scrambled siRNA + SHH
Ankmy2 siRNA
Ankmy2 siRNA + SHH

Figure 5

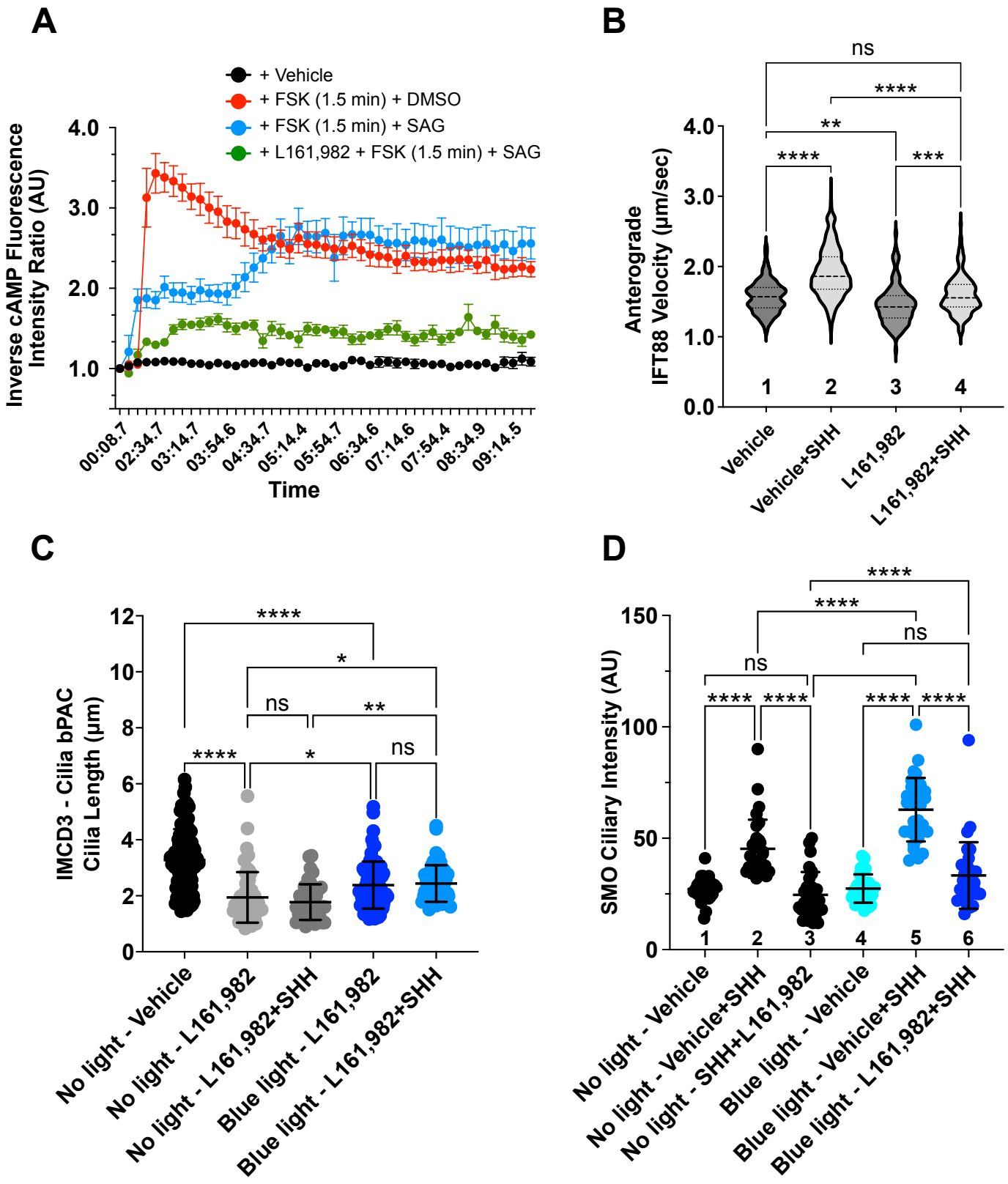
A
+ Vehicle
+ FSK (1.5 min) + DMSO
+ FSK (1.5 min) + SAG
+ L161,982 + FSK (1.5 min) + SAG
Inverse cAMP Fluorescence Intensity Ratio (AU)
4.0
3.0
2.0
1.0
00:08.7
02:34.7
03:14.7
03:54.6
04:34.7
05:14.4
05:54.7
06:34.6
07:14.6
07:54.4
08:34.9
09:14.5
Time
B
ns
****
**
****
***
Anterograde IFT88 Velocity (µm/sec)
4.0
3.0
2.0
1.0
0.0
1
2
3
4
Vehicle
Vehicle+SHH
L161,982
L161,982+SHH
C
****
*
ns
**
****
*
ns
IMCD3 - Cilia bPAC Cilia Length (µm)
12
10
8
6
4
2
0
No light - Vehicle
No light - L161,982
No light - L161,982+SHH
Blue light - L161,982
Blue light - L161,982+SHH
D
****
****
ns
ns
****
****
****
****
SMO Ciliary Intensity (AU)
150
100
50
0
1
2
3
4
5
6
No light - Vehicle
No light - Vehicle+SHH
No light - SHH+L161,982
Blue light - Vehicle
Blue light - Vehicle+SHH
Blue light - L161,982+SHH

Figure 6

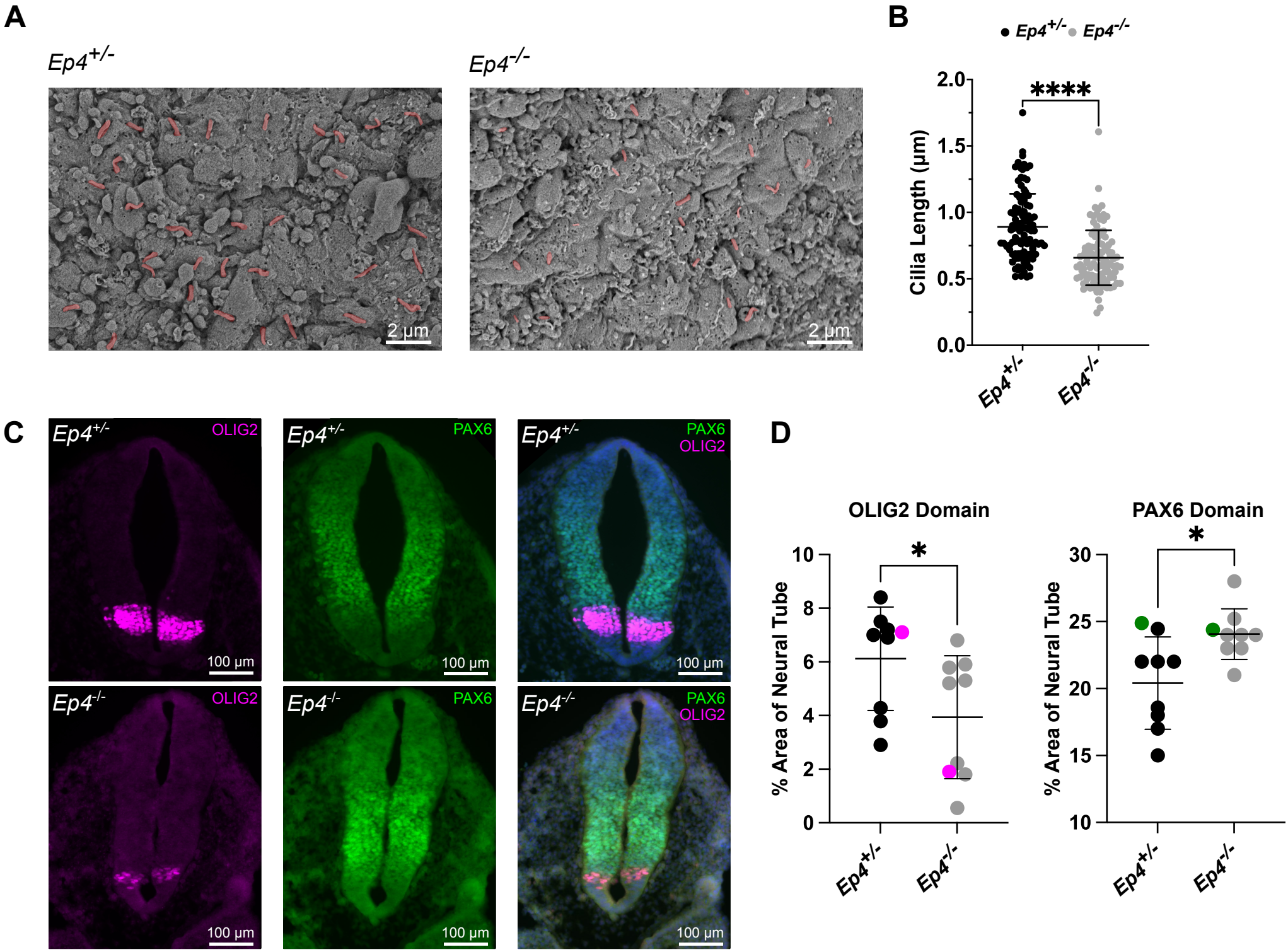
A
Ep4+/-
Ep4-/-
2 µm
2 µm
B
Ep4+/- Ep4-/-
Cilia Length (µm)
2.0
1.5
1.0
0.5
0.0
****
Ep4+/-
Ep4-/-
C
Ep4+/-
OLIG2
PAX6
PAX6
OLIG2
Ep4-/-
100 µm
D
OLIG2 Domain
PAX6 Domain
% Area of Neural Tube
*
*
10
8
6
4
2
0
30
25
20
15
10
Ep4+/-
Ep4-/-

Figure 7

A

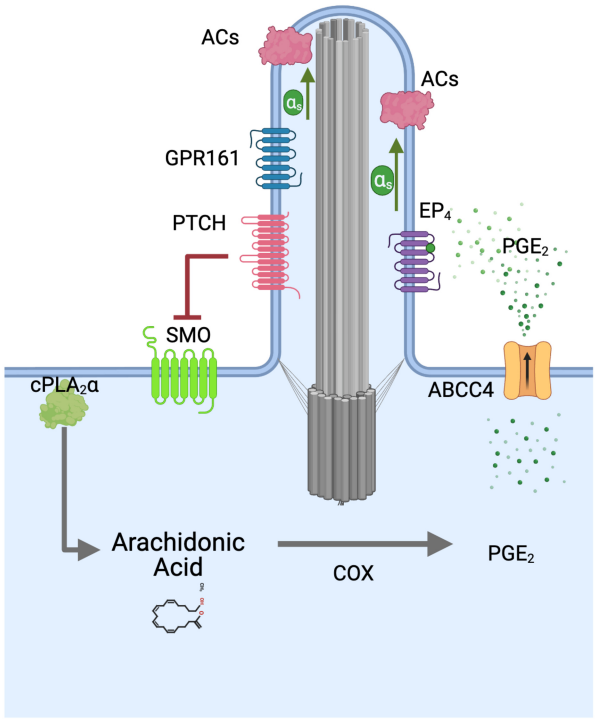

SHH Pathway OFF

GPR161 signaling to $G\alpha_s$

No SMO signaling to $G\alpha_i$ or GLI

Basal PGE_2/EP_4 signaling to $G\alpha_s$

Basal [cAMP]

B

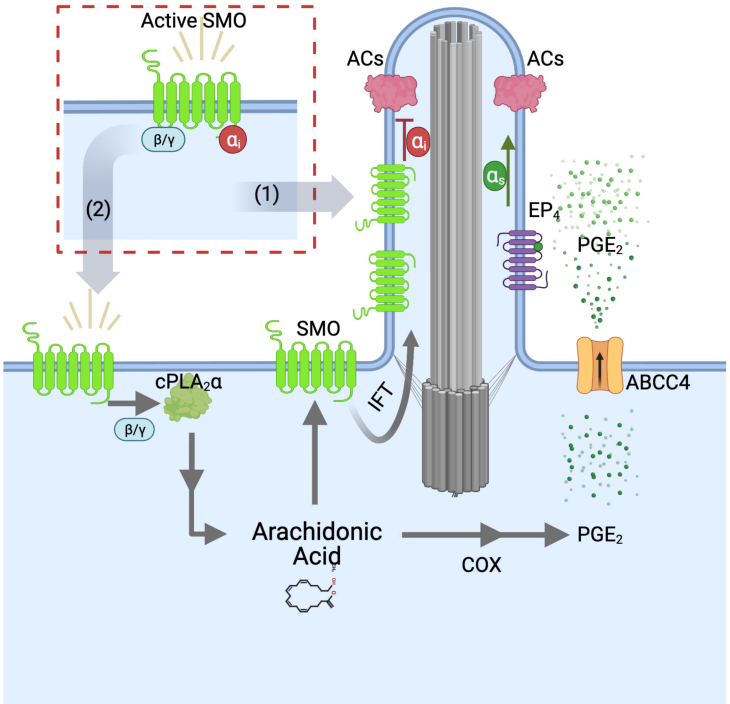

C

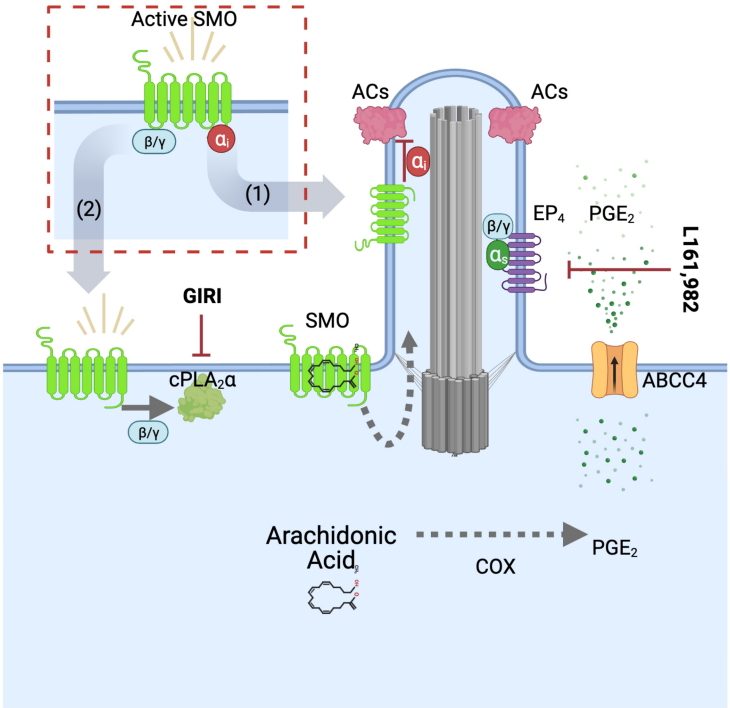

SHH Pathway ON

GPR161 exits cilia

SMO signaling to $G\alpha_i$ active

High SMO ciliary enrichment

High SMO signaling to GLI

Increased EP_4 signaling to $G\alpha_s$

[cAMP] equilibration

SHH Pathway ON +$cPLA_2$ or EP_4 inhibition

GPR161 exits cilia

SMO signaling to $G\alpha_i$ active

Decreased SMO ciliary enrichment

Attenuated SMO signaling to GLI

EP_4 signaling to $G\alpha_s$ inhibited

Disrupted [cAMP] equilibration

Supplementary Figure 1

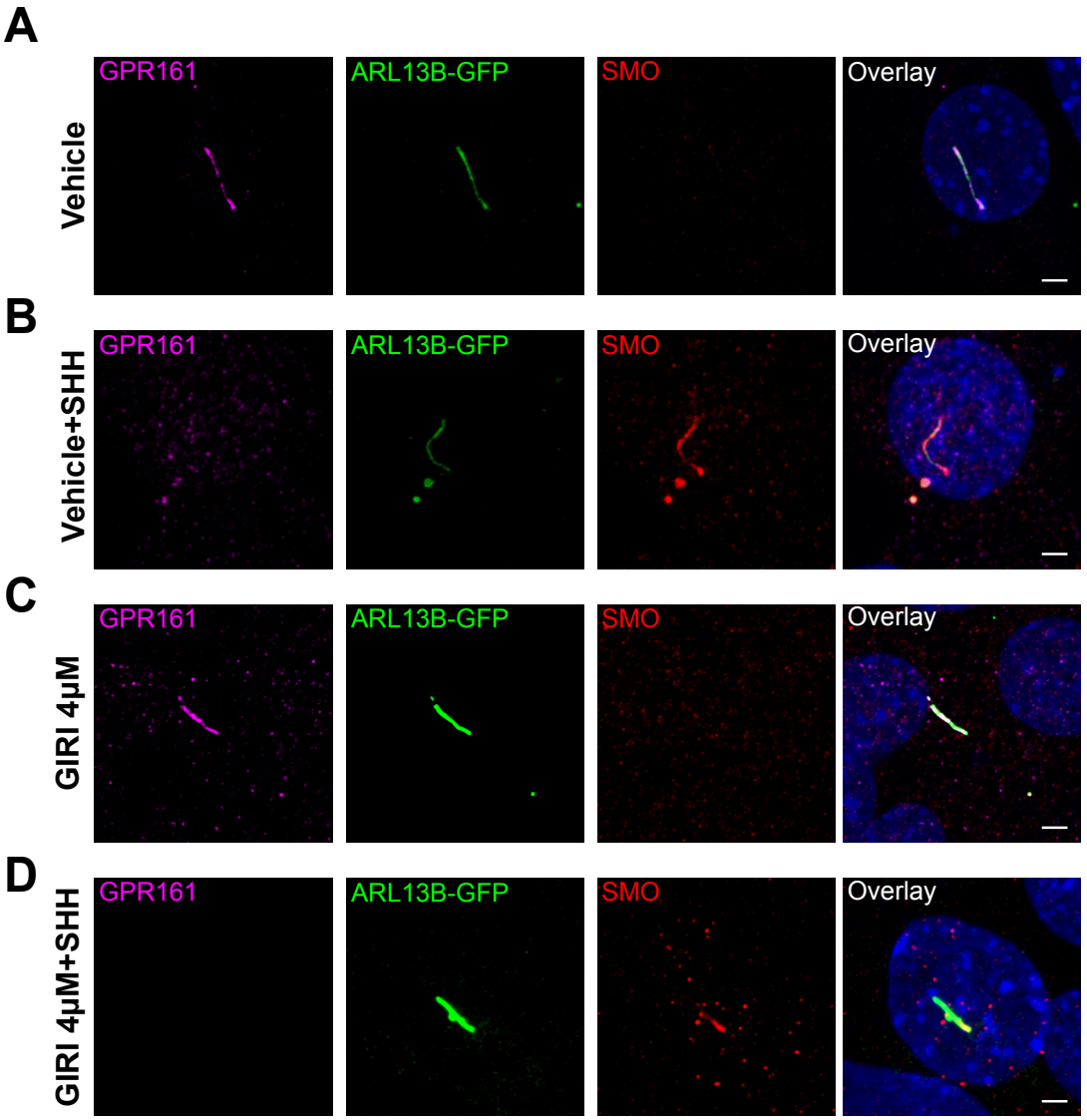

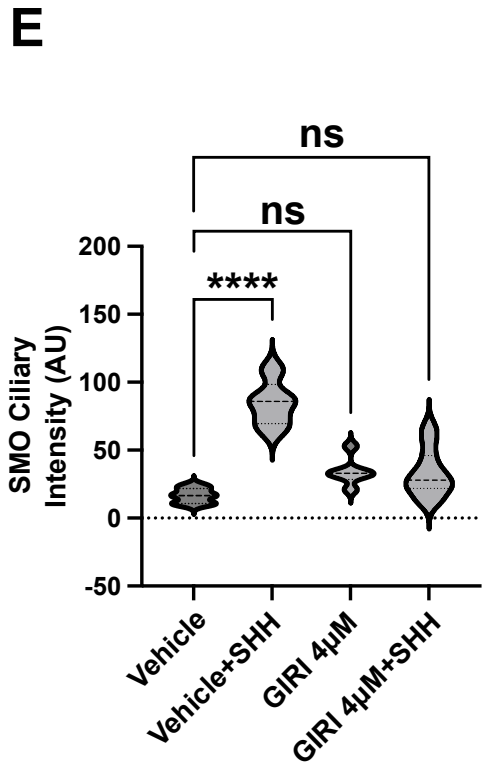

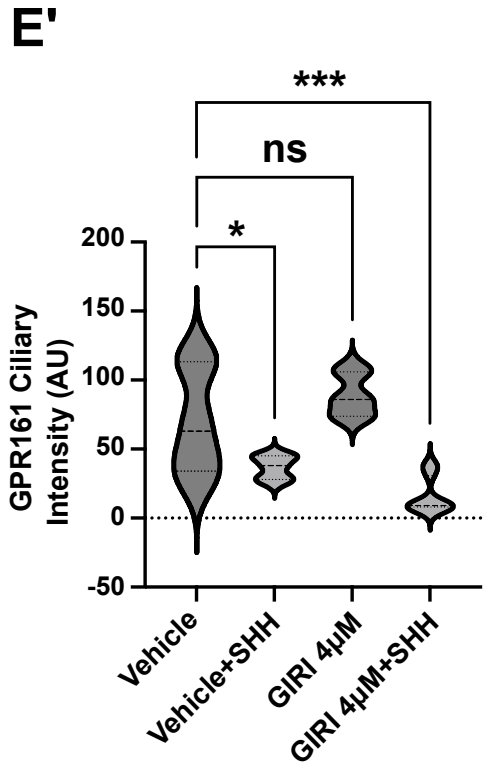

Supplementary Figure 2

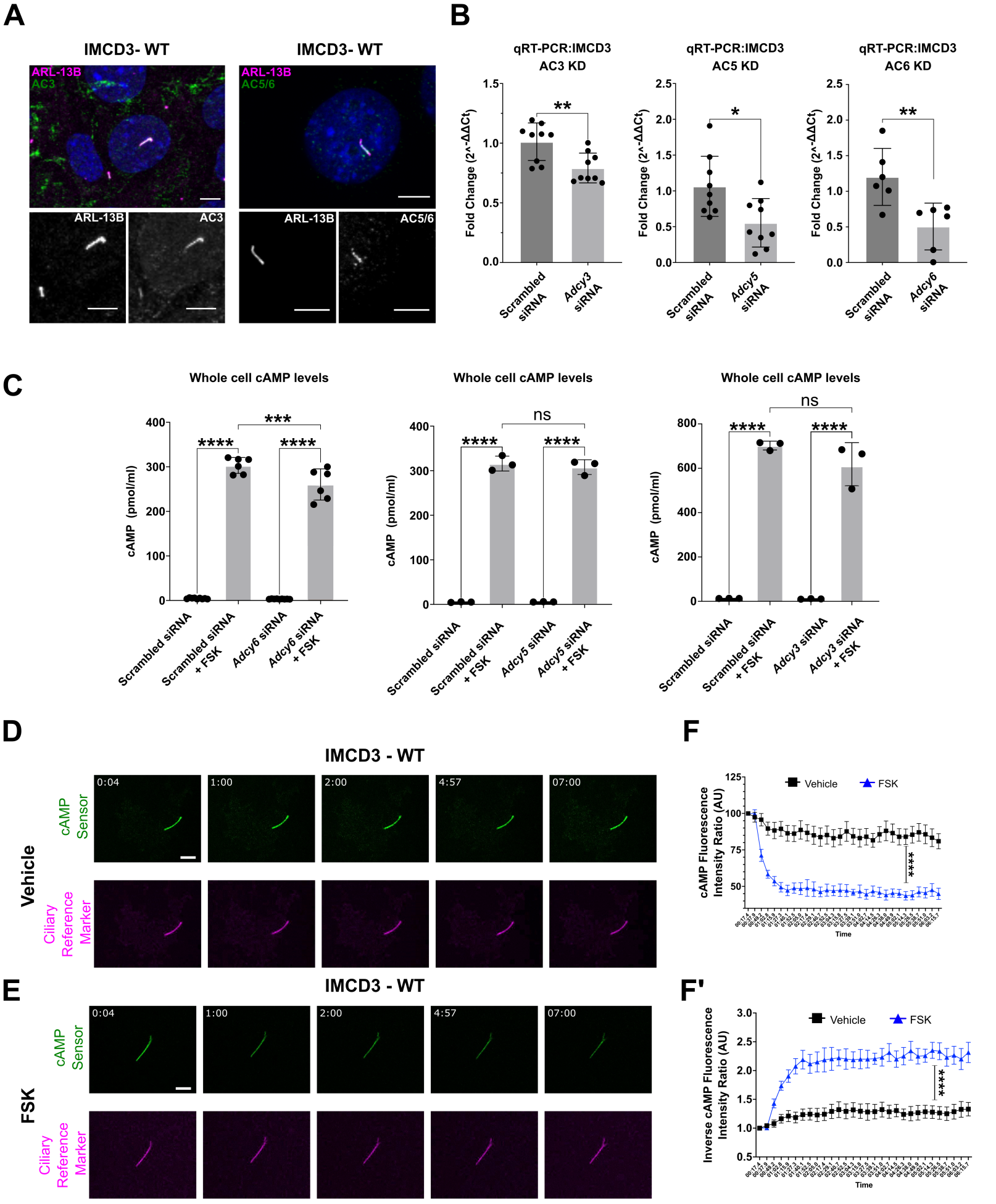

Supplementary Figure 3

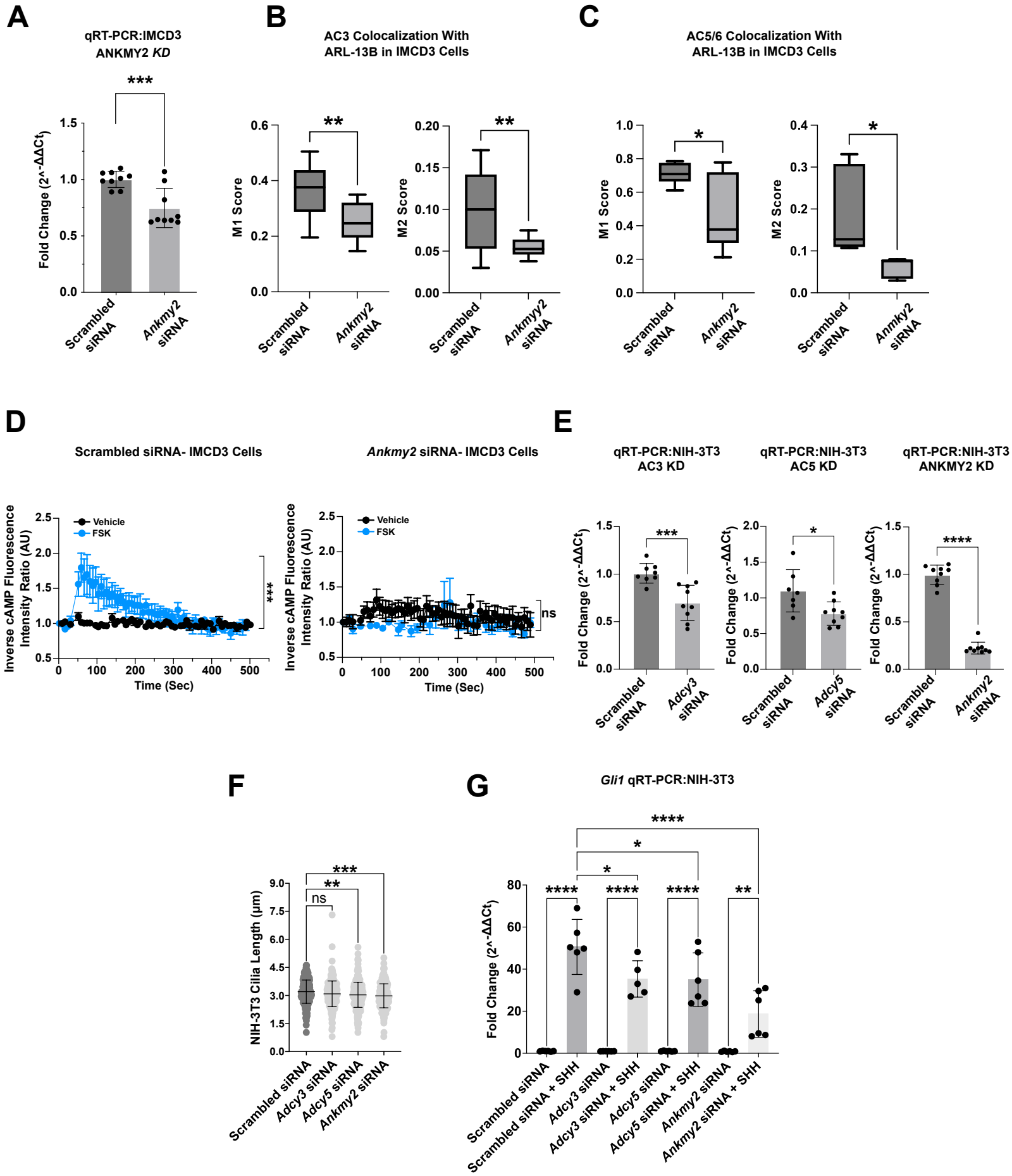
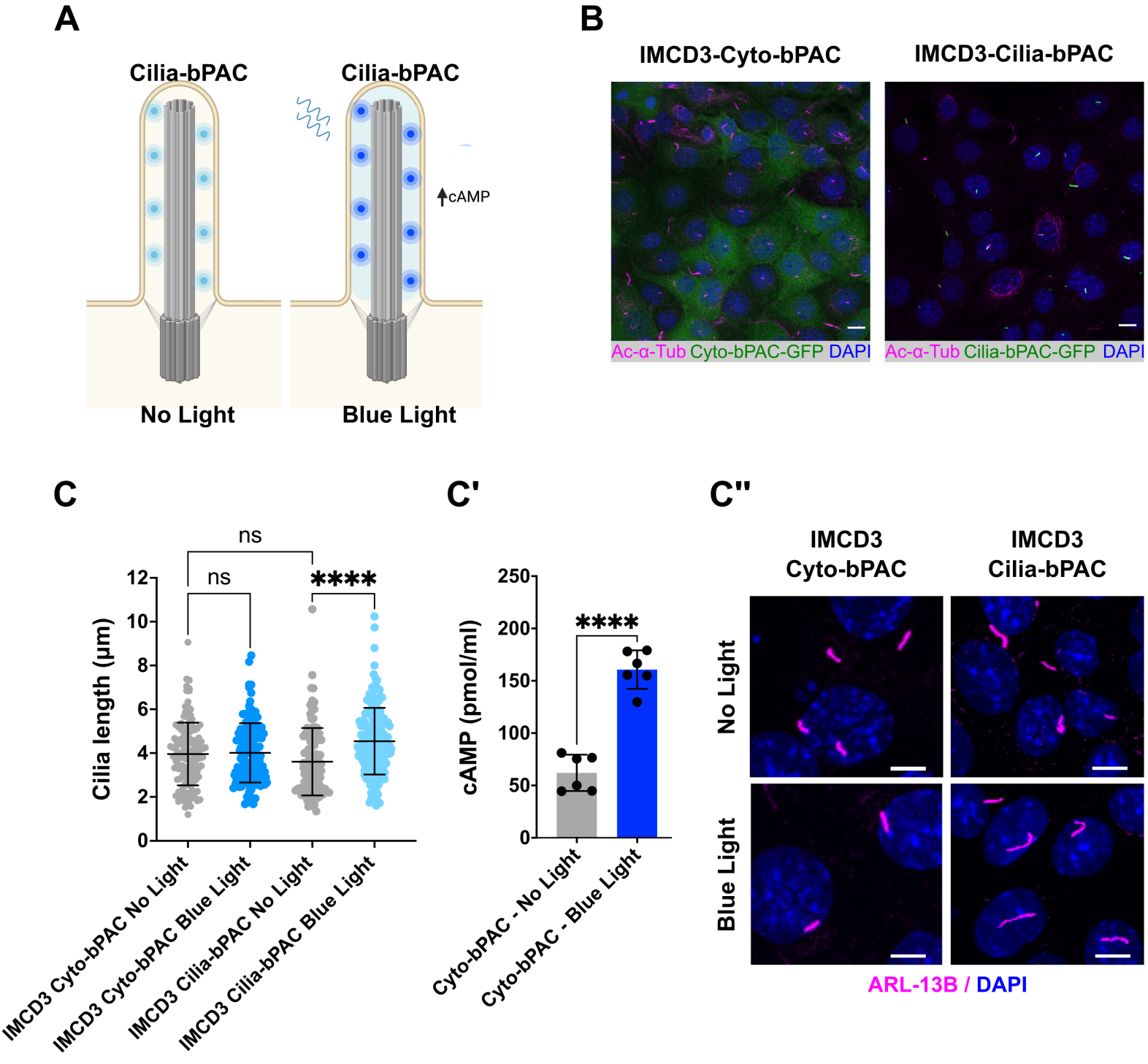
Supplementary Figure 4